An Efficient Approach for Dynamic-Reliability-Based Topology Optimization of Braced Frame Structures with Probability Density Evolution Method

Jia-Shu Yang, Ph.D. student

State Key Laboratory of Disaster Reduction in Civil Engineering & College of Civil Engineering, Tongji University, Shanghai 200092, P. R. China

E-mail: jiashuyang@tongji.edu.cn

Jian-Bing Chen (corresponding author)

Ph.D., University Distinguished Professor

State Key Laboratory of Disaster Reduction in Civil Engineering & College of Civil Engineering, Tongji University, Shanghai 200092, P. R. China

E-mail: chenjb@tongji.edu.cn

Michael Beer

Ph.D., Professor

Institute for Risk and Reliability, Leibniz Universität Hannover, Germany & Institute for Risk and Uncertainty, University of Liverpool, UK

Email: beer@irz.uni-hannover.de

Hector Jensen

Ph.D., Professor

Department of Civil Engineering, Federico Santa Maria Technical University, Valparaiso, Chile

E-mail: hector.jensen@usm.cl

Abstract

The present paper explores the feasibility of topology optimization of stochastic dynamical systems in the framework of the probability density evolution method (PDEM). A new method is proposed for solving dynamic-reliability-based topology optimization (DRBTO) problems by combining the PDEM, the ground structure approach and the solid isotropic material with penalization (SIMP) model. In the investigated optimization problems, the first-passage probability is considered as an objective or constraint function. To obtain a clear layout of the optimized structure, the topology of the structure is described by the ground structure approach together with the SIMP model. The PDEM is employed as an efficient approach to assess the first-passage probability. For improved numerical efficiency, an approximate formulation of the first-passage probability based on the important representative points (IRPs) is implemented. On the basis of the approximate formulation of the first-passage probability, a relationship between the sensitivity of the first-passage probability and the transient response is obtained. The adjoint sensitivity analysis of the transient response is introduced to avoid extra numerical efforts. Then, by incorporating the first-passage probability and its sensitivity into the method of moving asymptotes (MMA), the investigated DRBTO problems are solved in an effective manner. The DRBTO of a braced frame structure is presented to demonstrate the availability and effectiveness of the proposed method.

Keywords: first-passage probability, topology optimization, probability density evolution method, sensitivity analysis, braced frame structure

1. Introduction

Topology optimization is a powerful conceptual design methodology that can explore a complex design space to identify the set of most efficient structural configurations fulfilling prescribed requirements [1]. Extensive research on topology optimization has been carried out in the past few decades [2]. Besides, topology optimization has also been applied to a wide variety of structural systems, including continuum and discrete structures under static loads and dynamic excitations. For structures under dynamic excitations, topology optimization problems involving transient responses (e.g. peak values of dynamic responses) or vibration properties (e.g. natural frequencies) have also been investigated [3-5].

Despite the success of topology optimization, most of the research efforts in this field have focused on deterministic scenarios. Nonetheless, uncertainties in material properties and external excitations are inevitable in real-world engineering structural systems, and they usually have a significant effect on structural responses [6]. Thus, it is of practical significance to consider uncertainties in topology optimization. In this regard, two different frameworks have been developed. The first one is robust topology optimization (RTO) which aims at minimizing the sensitivity of structural performance with respect to uncertainties [7]. In the RTO framework, the objective function is usually defined as a combination of the mean value and standard deviation of the structural response of interest [8, 9]. The second framework is reliability-based topology optimization (RBTO), where reliability measures are included as part of the objective or constraint functions [10, 11]. Although the two frameworks are both instructive, RBTO is suitable for handling uncertainties in a probabilistic manner.

Under the framework of RBTO, a number of methods have been reported. In this regard, some of the traditional approaches for general reliability-based design optimization (RBDO), such as the double-loop method [12], the KKT condition-based single-loop method [13] and the sequential optimization and reliability assessment method [14], have been successfully extended to RBTO in the context of static structural systems [10, 15, 16]. Noting that most of these methods are developed based on the first-order reliability method (FORM), the extension to RBTO under dynamic scenarios becomes troublesome due to the inherent limitations of FORM [17].

Dynamic excitations, such as earthquakes and winds, usually play a dominant role in the structural design phase. Thus, it is indispensable to consider RBTO of structures subjected to dynamic excitations. Hence, dynamic-reliability-based-topology optimization (DRBTO), as a subclass of RBTO, requires especial attention. The paramount difference between topology optimization and standard design optimization is that the number of design variables in topology optimization is usually large [1]. This feature hinders the application of methods for general dynamic-reliability-based design optimization (DRBDO) in topology optimization. It is noted that, for general DRBDO problems, the number of design variables is generally restricted to a small number [18]. On the other hand, the first-passage probability is a commonly used measure for dynamic reliability [19], and consequently, it is usually involved in DRBTO problems as a part of the objective or constraint functions. However, calculating the first-passage probability has become a persistent challenge for more than half a century. A number of approaches, such as methods based on the out-crossing rates [20], methods which solve the backward Kolmogorov equation or the Chapman-Kolmogorov equation considering absorbing boundary conditions [21-23], have been developed to evaluate the first-passage probability of various dynamical systems. Nevertheless, difficulties still exist, especially for problems involving high-dimensional systems. This fact makes the solution of DRBTO problems quite challenging.

Compared to RBTO under static loads, relatively few investigations have been reported in DRBTO.

In Xu et al. [24] and Hu et al. [25], first-passage probability measures were approximated in terms of the out-crossing rates of the responses of interest, which assumes a Poisson distribution for the out-crossing events [26]. Similarly, Chun et al. [27] employed FORM with the sequential compounding method to approximate the first-passage probability. These approaches have mostly focused on linear structural systems under stationary or nonstationary Gaussian excitation using ad-hoc procedures for reliability sensitivity assessment. In general, their accuracy is problem-dependent due to the approximate nature of the underlying reliability assessment techniques. On the other hand, Bobby et al. [28] implemented a sequential optimization approach. During each optimization cycle, reliability constraints are approximated in terms of equivalent threshold constraints using information from direct Monte Carlo simulation (MCS). Although the technique can handle linear structures subjected to general stochastic excitations, the associated computational efforts can be significant or even prohibitive for highly reliable systems. From the previous discussion, available techniques for DRBTO can address different types of problems with different levels of effectiveness. Thus, there is still room for further developments in this area, especially regarding the integration of efficient reliability and reliability sensitivity assessment techniques.

As previously pointed out, the dynamic reliability analyses and the corresponding sensitivity analyses account for most of the computational efforts in DRBTO. Thus, an efficient dynamic reliability analysis is of particular importance. In this context, the probability density evolution method (PDEM) [19, 29], which has experienced promising developments in recent years, provides an alternative choice. In the present paper, the feasibility of solving DRBTO problems within the framework of the PDEM is explored. Specifically, a method for DRBTO is proposed by incorporating the PDEM with the solid isotropic material with penalization (SIMP) [30] model and the ground structure approach [31]. The DRBTO problem of braced frame structures is further investigated using the proposed method. The topology of braced frame structures is implemented using the ground structure approach and the SIMP models. The PDEM is adopted to assess the first-passage probability, and a strategy for approximate dynamic reliability analysis is introduced based on the concept of important representative points (IRPs) [32]. The sensitivity of the first-passage probability is derived such that a class of first-order optimizer, namely, the method of moving asymptotes (MMA) [33], can be adopted to solve the corresponding optimization problems. In addition, the adjoint sensitivity analysis of structural transient response is introduced to speed-up the design sensitivity analysis of the first-passage probability.

The rest of the present paper is organized as follows: Section 2 presents the general formulation of DRBTO. The PDEM as a dynamic reliability analysis method is briefly outlined in Section 3. In addition, an approximate formulation of the first-passage probability is derived. The sensitivity analysis of the first-passage probability is introduced in Section 4. In Section 5, some implementation aspects are discussed, and an overall procedure of the proposed method is provided. In Section 6, numerical examples are presented to verify the effectiveness of the proposed method. Some final remarks and future research efforts are provided in Section 7.

2. Formulation of DRBTO Problem

2.1. Topology Optimization Framework

Topology optimization problems of truss or frame structures are usually formulated in terms of the ground structure method [31]. In this approach, a set of fixed nodes are first determined and the ground structure is given by a set of members which densely connect the fixed nodes. By allowing ground structure members to vanish, topology optimization tries to identify the remaining members in the final design.

Generally, topology optimization of truss structures treats the section areas of ground structure members as design variables. By setting the section areas of some members to be zero, the topology of the structure is changed. In this formulation, the topology optimization problem is converted into a standard size optimization problem. Noting that the section areas of members can continuously vary in a given range, this formulation simultaneously optimizes the size and topology of a given truss structure [1]. Another approach is to introduce independent binary design variables controlling the existence of the members. To avoid the difficulty of solving a large scale 0-1 integer programming problem, the design variables are relaxed to be continuous in the interval $[0,1]$. Then, intermediate values of the design variables are penalized, such that an approximate binary solution is obtained. In this context, the SIMP model [30], which has been generally used for topology optimization of continua, can also be used for problems involving frame or truss structures [25, 34, 35]. When the SIMP model is adopted in the topology optimization of frame or truss structures, the section sizes of the members remain constant, but only the existence states are switched. One of the advantages of this approach is that the optimized structures can be easily manufactured since the remaining members are of uniform section sizes [34].

In the previous context, the design variables, interpreted as element densities, are penalized by a power function to avoid intermediate values. In particular, the elastic modulus of the e-th element is given by

$$E(x_e) = E_{\min} + x_e{}^p (E_0 - E_{\min}) \tag{1}$$

where $x_e \in [0,1]$ is the design variable, i.e., density of the e-th element; $E_{\min}$ is a small positive value of the void element to circumvent singularity; $p > 1$ denotes the penalization parameter; and E_0 is the original elastic modulus of the material. Note that the physical material density remains constant. In this way, the stiffness and mass matrices of the e-th element (with element density x_e) are respectively given by

$$\mathbf{k}_e(x_e) = \kappa \mathbf{k}_{e,0} + x_e{}^p (1-\kappa)\mathbf{k}_{e,0} \tag{2}$$

$$\mathbf{m}_e(x_e) = \kappa \mathbf{m}_{e,0} + x_e (1-\kappa)\mathbf{m}_{e,0} \tag{3}$$

where $\mathbf{k}_{e,0}$ and $\mathbf{m}_{e,0}$ are the original stiffness and mass matrices of the e-th element with full attributes, respectively; and $\kappa = E_{\min}/E_0$. Accordingly, the sensitivity of $\mathbf{k}_e$ and $\mathbf{m}_e$ with respect to x_e are given by

$$\frac{\partial \mathbf{k}_e(x_e)}{\partial x_e} = p x_e{}^{p-1}(1-\kappa)\mathbf{k}_{e,0} \tag{4}$$

$$\frac{\partial \mathbf{m}_e}{\partial x_e}(x_e) = (1-\kappa)\mathbf{m}_{e,0} \tag{5}$$

In the present implementation, the value of κ is taken as 1×10^{-4}.

The global stiffness matrix $\mathbf{K}$ and the global mass matrix $\mathbf{M}$ of the structure are obtained by assembling $\mathbf{k}_e$ and $\mathbf{m}_e$ of all elements as in the standard finite element procedure. In addition, the Rayleigh damping matrix is considered as $\mathbf{C} = a_0\mathbf{M} + a_1\mathbf{K}$, where a_0 and a_1 are the proportionality coefficients.

2.2. First-Passage Probability

Consider a linear stochastic dynamical system of m degrees of freedom (DOFs):

$$\mathbf{M}(\boldsymbol{\Theta};\mathbf{x})\ddot{\mathbf{Y}} + \mathbf{C}(\boldsymbol{\Theta};\mathbf{x})\dot{\mathbf{Y}} + \mathbf{K}(\boldsymbol{\Theta};\mathbf{x})\mathbf{Y} = \mathbf{f}(\boldsymbol{\Theta},t;\mathbf{x}) \tag{6}$$

where $\boldsymbol{\Theta} = (\Theta_1, \Theta_2, \cdots, \Theta_N)^{\mathrm{T}}$ is the N-dimensional vector of random variables; $\mathbf{x} = (x_1, x_2, \cdots, x_n)^{\mathrm{T}}$ is the n-dimensional vector of design variables; $\mathbf{M}$, $\mathbf{C}$ and $\mathbf{K}$ are the $m\times m$ global mass, damping and stiffness matrices of the system, respectively; $\mathbf{Y}$, $\dot{\mathbf{Y}}$ and $\ddot{\mathbf{Y}}$ are the m-dimensional displacement, velocity and acceleration response vectors, respectively; $\mathbf{f}$ denotes the excitation vector; and t is the time variable. For seismic excitations, the vector $\mathbf{f}$ is defined by

$$\mathbf{f}(\boldsymbol{\Theta},t;\mathbf{x}) = -\mathbf{M}(\boldsymbol{\Theta};\mathbf{x})\boldsymbol{\iota}\ddot{u}_g(\boldsymbol{\Theta},t) \tag{7}$$

where $\boldsymbol{\iota}$ is an m-dimensional influence vector, and $\ddot{u}_g$ is the seismic ground acceleration. Note that, in $\boldsymbol{\iota}$, only the entries corresponding to the DOFs in the direction of the ground motion are one, while the other entries are zero [36]. For the numerical solution of the equation of motion, the Newmark-β method with a constant time step size is employed. In particular, the constant average acceleration method which is unconditionally stable is used. In this setting, the time step size is denoted by h and the discretized time series by $t_1, t_2, \cdots, t_{N_{\mathrm{T}}}$, where $t_i = ih,\ i = 1, 2, \cdots, N_{\mathrm{T}}$.

For stochastic dynamical systems, the first-passage probability is a common and practical measure of reliability [19]. Hence, DRBTO problems are formulated in terms of the first-passage probability in this work.

In this framework, denote the structural response of interest by Z which can be defined in terms of the displacement, velocity and acceleration vectors. Then, the normalized extreme value of Z is defined as

$$Z_{\text{ext}}(\boldsymbol{\Theta};\mathbf{x}) = \max_{t\in[0,T]}\left\{\left|\frac{Z(\boldsymbol{\Theta},t;\mathbf{x})}{z^{\text{th}}}\right|\right\} \tag{8}$$

where $[0,T]$ denotes the time interval of analysis; and z^{th} is the threshold of Z. The first-passage probability related to Z, for a given design $\mathbf{x}$, is given by

$$P_{\text{F}}(\mathbf{x}) = \Pr\{Z_{\text{ext}}(\boldsymbol{\Theta};\mathbf{x}) > 1\} \tag{9}$$

2.3. Optimization Problem Formulation

In the present paper, two formulations of DRBTO problems are considered. In the first formulation, the first-passage probability is minimized under a constraint on material volume. Specifically, the problem is formulated as

$$\begin{aligned} &\min \ P_{\text{F}}(\mathbf{x}) \\ &\text{s.t.} \ \mathbf{x}^{\mathsf{T}}\mathbf{v} \le \overline{v} \\ &\qquad \mathbf{M}(\boldsymbol{\Theta};\mathbf{x})\ddot{\mathbf{Y}} + \mathbf{C}(\boldsymbol{\Theta};\mathbf{x})\dot{\mathbf{Y}} + \mathbf{K}(\boldsymbol{\Theta};\mathbf{x})\mathbf{Y} = \mathbf{f}(\boldsymbol{\Theta},t;\mathbf{x}) \\ &\qquad x_e \in [0,1], e = 1,2,\cdots,n \end{aligned} \tag{10}$$

where $\mathbf{x}$ is the vector of design variables (element densities); $P_{\text{F}}(\mathbf{x})$ denotes the first-passage probability function as defined in Section 2.2; $\mathbf{v} = (v_1, v_2, \cdots, v_n)^{\mathsf{T}}$ is the n-dimensional vector of element volumes in which v_e is the volume of the e-th element; $\overline{v}$ denotes the maximum allowable material volume; and n is the number of design variables.

In the second formulation, the material volume is minimized while a constraint on the first-passage probability is included. In particular, the problem is given by

$$\begin{aligned} &\min \ V(\mathbf{x}) = \mathbf{x}^{\mathsf{T}}\mathbf{v} \\ &\text{s.t.} \ P_{\text{F}}(\mathbf{x}) \le P_{\text{F}}^{\text{th}} \\ &\qquad \mathbf{M}(\boldsymbol{\Theta};\mathbf{x})\ddot{\mathbf{Y}} + \mathbf{C}(\boldsymbol{\Theta};\mathbf{x})\dot{\mathbf{Y}} + \mathbf{K}(\boldsymbol{\Theta};\mathbf{x})\mathbf{Y} = \mathbf{f}(\boldsymbol{\Theta},t;\mathbf{x}) \\ &\qquad x_e \in [0,1], e = 1,2,\cdots,n \end{aligned} \tag{11}$$

where $V(\mathbf{x})$ is the material volume function, and P_{F}^{th} is the allowable probability of failure.

3. Dynamic Reliability Analysis

The PDEM together with the equivalent extreme value distribution [37] is employed for dynamic reliability analysis in the present paper. Thereby, for clarity, a brief introduction to the PDEM is first outlined in this section. Moreover, in order to further enhance the efficiency of dynamic reliability analysis, an approximate formulation of the first-passage probability is derived.

3.1. PDEM-based Dynamic Reliability Analysis

Consider a stochastic dynamical system governed by Eq.(6). If the system is well-posed, the solution of the system uniquely exists, and it depends on the design vector $\mathbf{x}$, the random vector $\mathbf{\Theta}$, the time variable t, and the initial condition. Since the structural response of interest, i.e., Z, is a differentiable function of the solution of the stochastic dynamical system, it can also be uniquely determined.

Noting that all random factors involved in the stochastic dynamical system are characterized by the random vector $\mathbf{\Theta}$, the $(N+1)$-dimensional augmented system $(Z,\mathbf{\Theta})$ is probability-preserved. Due to the principle of preservation of probability [38], the one-dimensional generalized density evolution equation (GDEE) which governs the evolution of the joint probability density function (PDF) of the augmented system takes the form

$$\frac{\partial p_{Z\mathbf{\Theta}}(z,\boldsymbol{\theta},t;\mathbf{x})}{\partial t}+\dot{Z}(\boldsymbol{\theta},t;\mathbf{x})\frac{\partial p_{Z\mathbf{\Theta}}(z,\boldsymbol{\theta},t;\mathbf{x})}{\partial z}=0 \tag{12}$$

where $\boldsymbol{\theta}=(\theta_1,\theta_2,\cdots,\theta_N)^{\mathsf{T}}$ is a realization of $\mathbf{\Theta}$, z is a realization of Z; and $p_{Z\mathbf{\Theta}}(z,\boldsymbol{\theta},t;\mathbf{x})$ denotes the joint PDF of Z and $\mathbf{\Theta}$ at a given time t and design $\mathbf{x}$. The initial condition of Eq.(12) is

$$p_{Z\mathbf{\Theta}}(z,\boldsymbol{\theta},t;\mathbf{x})\big|_{t=0}=\delta(z-z_0)\,p_{\mathbf{\Theta}}(\boldsymbol{\theta}) \tag{13}$$

where z_0 is the initial value of Z, $\delta(\cdot)$ denotes Dirac's delta function; and $p_{\mathbf{\Theta}}(\boldsymbol{\theta})$ is the joint PDF of the random vector $\mathbf{\Theta}$. Herein, z_0 is independent of both $\mathbf{x}$ and $\mathbf{\Theta}$. For the theoretical aspects and the physical interpretation of the GDEE, readers can refer to Li and Chen [19].

The PDEM can serve as an efficient method to assess the first-passage probability when combined with the equivalent extreme value distribution strategy [37]. In this framework, a virtual stochastic process is defined as [33]

$$W(\mathbf{\Theta},\tau;\mathbf{x})=Z_{\mathrm{ext}}(\mathbf{\Theta};\mathbf{x})\sin\left(\frac{5\pi}{2}\tau\right) \tag{14}$$

where Z_{ext} is the normalized extreme value of Z defined in Eq.(8), and τ is a virtual time variable. The form of the virtual stochastic process is not unique, and the basic guidelines for constructing a virtual stochastic process can be found in Li et al. [37] and Li and Chen [19]. In principle, the form of the virtual stochastic process has a limited effect on the dynamic reliability. The present formulation considers the sine-type virtual stochastic process following Li et al. [37], since validation calculations indicate that a sine-type virtual stochastic process can usually lead to a precise first-passage probability estimate.

Note that $(W, \boldsymbol{\Theta})$ forms a probability-preserved system. Similar to Eq.(12), the GDEE governing the evolution of the joint PDF of the augmented system $(W, \boldsymbol{\Theta})$ is written as

$$\frac{\partial p_{W\boldsymbol{\Theta}}(w, \boldsymbol{\theta}, \tau; \mathbf{x})}{\partial \tau} + \dot{W}(\boldsymbol{\theta}, \tau; \mathbf{x}) \frac{\partial p_{W\boldsymbol{\Theta}}(w, \boldsymbol{\theta}, \tau; \mathbf{x})}{\partial w} = 0 \tag{15}$$

where $\dot{W}(\boldsymbol{\theta}, \tau; \mathbf{x}) = 5\pi/2 \cdot Z_{\text{ext}}(\boldsymbol{\theta}; \mathbf{x}) \cos(5\pi\tau/2)$, and $p_{W\boldsymbol{\Theta}}(w, \boldsymbol{\theta}, \tau; \mathbf{x})$ is the joint PDF of W and $\boldsymbol{\Theta}$. Accordingly, the initial condition of Eq.(15) is

$$p_{W\boldsymbol{\Theta}}(w, \boldsymbol{\theta}, \tau; \mathbf{x})\big|_{\tau=0} = \delta(w)\, p_{\boldsymbol{\Theta}}(\boldsymbol{\theta}) \tag{16}$$

Since $W(\boldsymbol{\Theta}, \tau; \mathbf{x})$ is identical to $Z_{\text{ext}}(\boldsymbol{\Theta}; \mathbf{x})$ when $\tau = 1$, the joint PDF of Z_{ext} and $\boldsymbol{\Theta}$, namely, $p_{Z_{\text{ext}}\boldsymbol{\Theta}}$, is given by

$$p_{Z_{\text{ext}}\boldsymbol{\Theta}}(z, \boldsymbol{\theta}; \mathbf{x}) = p_{W\boldsymbol{\Theta}}(w = z, \boldsymbol{\theta}, \tau; \mathbf{x})\big|_{\tau=1} \tag{17}$$

where z is a realization of Z_{ext}.

By solving Eq.(15), $p_{W\boldsymbol{\Theta}}(w, \boldsymbol{\theta}, \tau; \mathbf{x})$ and thereby $p_{Z_{\text{ext}}\boldsymbol{\Theta}}(z, \boldsymbol{\theta}; \mathbf{x})$ are obtained. Integrating $p_{Z_{\text{ext}}\boldsymbol{\Theta}}(z, \boldsymbol{\theta}; \mathbf{x})$ over the probability space of $\boldsymbol{\Theta}$, i.e., $\Omega_{\boldsymbol{\Theta}}$, yields the PDF of Z_{ext}:

$$p_{Z_{\text{ext}}}(z; \mathbf{x}) = \int_{\Omega_{\boldsymbol{\Theta}}} p_{Z_{\text{ext}}\boldsymbol{\Theta}}(z, \boldsymbol{\theta}; \mathbf{x})\, \mathrm{d}\boldsymbol{\theta} \tag{18}$$

Finally, the first-passage probability, i.e., the probability of failure, is given by a one-dimensional integral of $p_{Z_{\text{ext}}}(z; \mathbf{x})$ over the failure interval of Z_{ext}, that is

$$P_{\text{F}}(\mathbf{x}) = \int_{1}^{+\infty} p_{Z_{\text{ext}}}(z; \mathbf{x})\, \mathrm{d}z_{\text{ext}} \tag{19}$$

For most practical systems, the closed-form solution of the GDEE is not available. Thus, the GDEE is usually solved by numerical methods. For completeness, a general solution procedure for the PDEM-based dynamic reliability analysis is outlined in Appendix I.

3.2. Dynamic Reliability Analysis at Perturbed Designs

Although the PDEM-based method is efficient, the repeated dynamic reliability assessments involved in the optimization process still account for a large amount of computational efforts. Thus, an approximate formulation of the first-passage probability based on information obtained from the PDEM results is implemented in this work.

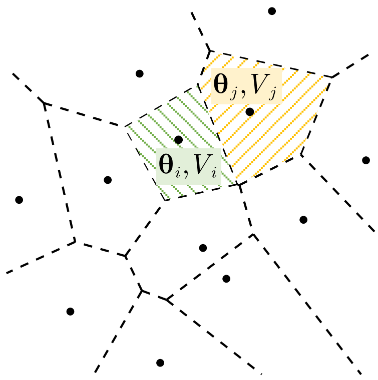

Fig. 1. Representative regions and points in a 2D probability space

In the implementation of the PDEM-based dynamic reliability analysis, the probability space $\Omega_{\boldsymbol{\Theta}}$ is first discretized into a series of representative regions which are specified by Voronoi cells [39]. Denote the representative regions by V_q, $q = 1, 2, \cdots, N_{\mathrm{R}}$, where N_{R} is the number of representative regions. In the q-th representative region, i.e., V_q, a representative point is selected and denoted by $\boldsymbol{\theta}_q$. The assigned probability of $\boldsymbol{\theta}_q$, namely, P_q, is defined as the integral of $p_{\boldsymbol{\Theta}}(\boldsymbol{\theta})$ over V_q (see Appendix I). Fig. 1 schematically shows the representative regions and points in a 2D probability space.

Noting that the representative regions, $\{V_q\}_{q=1}^{N_{\mathrm{R}}}$, form a partition of the probability space, the first-passage probability specified by Eq.(9) can be rewritten as

$$P_{\mathrm{F}}(\mathbf{x}) = \sum_{q=1}^{N_{\mathrm{R}}} \Pr\{Z_{\mathrm{ext}}(\boldsymbol{\Theta}; \mathbf{x}) > 1 \cap \boldsymbol{\Theta} \in V_q\} \tag{20}$$

where

$$\Pr\{Z_{\mathrm{ext}}(\boldsymbol{\Theta}; \mathbf{x}) > 1 \cap \boldsymbol{\Theta} \in V_q\} = \int_1^{+\infty} p_{Z_{\mathrm{ext}}}^{(q)}(z; \mathbf{x})\,\mathrm{d}z \tag{21}$$

in which $p_{Z_{\mathrm{ext}}}^{(q)}(z; \mathbf{x})$ is the solution of the GDEE associated with the q-th representative region when $\tau = 1$ at a given design $\mathbf{x}$ (see Appendix I).

Similarly, the first-passage probability at a perturbed design is cast as

$$P_{\mathrm{F}}(\mathbf{x} + \boldsymbol{\Delta}) = \sum_{q=1}^{N_{\mathrm{R}}} \Pr\{Z_{\mathrm{ext}}(\boldsymbol{\Theta}; \mathbf{x} + \boldsymbol{\Delta}) > 1 \cap \boldsymbol{\Theta} \in V_q\} \tag{22}$$

where $\boldsymbol{\Delta}$ is a small perturbation of the design vector. Denote the increment of Z_{ext} induced by the perturbation of the design vector by $D(\boldsymbol{\Theta}, \mathbf{x}, \boldsymbol{\Delta})$, that is,

$$D(\boldsymbol{\Theta}, \mathbf{x}, \boldsymbol{\Delta}) = Z_{\mathrm{ext}}(\boldsymbol{\Theta}; \mathbf{x} + \boldsymbol{\Delta}) - Z_{\mathrm{ext}}(\boldsymbol{\Theta}; \mathbf{x}) \tag{23}$$

Substituting Eq.(23) into Eq.(22) yields an equivalent formulation of the first-passage probability at $\mathbf{x} + \boldsymbol{\Delta}$:

$$P_{\mathrm{F}}(\mathbf{x}+\boldsymbol{\Delta})=\sum_{q=1}^{N_{\mathrm{R}}}\Pr\{Z_{\mathrm{ext}}(\boldsymbol{\Theta};\mathbf{x})>1-D(\boldsymbol{\Theta},\mathbf{x},\boldsymbol{\Delta})\cap\boldsymbol{\Theta}\in V_q\} \tag{24}$$

If a sufficient number of representative points are adopted in the numerical solution of the PDEM, the volume of each representative region will be relatively small. Accordingly, the assigned probability associated with a representative point will also be small. Thus, it is reasonable to ignore the variation of $D(\boldsymbol{\Theta},\mathbf{x},\boldsymbol{\Delta})$ in a representative region. As a result, one can replace $D(\boldsymbol{\Theta},\mathbf{x},\boldsymbol{\Delta})$ by the increment of Z_{ext} at the associated representative point at the expense of a small error [32], that is,

$$\forall\boldsymbol{\Theta}\in V_q,\ D(\boldsymbol{\Theta},\mathbf{x},\boldsymbol{\Delta})\approx D(\boldsymbol{\theta}_q,\mathbf{x},\boldsymbol{\Delta}) \tag{25}$$

By introducing Eq.(25) into Eq.(24), an estimate of the first-passage probability at the perturbed design is obtained:

$$\widehat{P_{\mathrm{F}}}(\mathbf{x}+\boldsymbol{\Delta})=\sum_{q=1}^{N_{\mathrm{R}}}\Pr\{Z_{\mathrm{ext}}(\boldsymbol{\Theta};\mathbf{x})>1-D(\boldsymbol{\theta}_q,\mathbf{x},\boldsymbol{\Delta})\cap\boldsymbol{\Theta}\in V_q\} \tag{26}$$

where $\widehat{P_{\mathrm{F}}}(\mathbf{x}+\boldsymbol{\Delta})$ is an estimate of $P_{\mathrm{F}}(\mathbf{x}+\boldsymbol{\Delta})$.

On the other hand, note that

$$\Pr\{Z_{\mathrm{ext}}(\boldsymbol{\Theta};\mathbf{x})>1-D(\boldsymbol{\theta}_q,\mathbf{x},\boldsymbol{\Delta})\cap\boldsymbol{\Theta}\in V_q\}=\int_{1-D^{(q)}}^{+\infty}p_{Z_{\mathrm{ext}}}^{(q)}(z;\mathbf{x})\,\mathrm{d}z \tag{27}$$

where $D^{(q)}=D(\boldsymbol{\theta}_q,\mathbf{x},\boldsymbol{\Delta})$. By substituting Eq.(27) into Eq.(26), the estimate of the first-passage probability at the perturbed design is reformulated in the form:

$$\widehat{P_{\mathrm{F}}}(\mathbf{x}+\boldsymbol{\Delta})=\sum_{q=1}^{N_{\mathrm{R}}}\int_{1-D^{(q)}}^{+\infty}p_{Z_{\mathrm{ext}}}^{(q)}(z;\mathbf{x})\,\mathrm{d}z \tag{28}$$

By combining Eqs.(20), (21) and (28), $\hat{P}_{\mathrm{F}}(\mathbf{x}+\boldsymbol{\Delta})$ is further recast as

$$\widehat{P_{\mathrm{F}}}(\mathbf{x}+\boldsymbol{\Delta})=P_{\mathrm{F}}(\mathbf{x})+\sum_{q=1}^{N_{\mathrm{R}}}\int_{1-D^{(q)}}^{1}p_{Z_{\mathrm{ext}}}^{(q)}(z;\mathbf{x})\,\mathrm{d}z \tag{29}$$

Validation calculations indicate that Eq.(29) can provide an approximation to the first-passage probability with high accuracy [32]. Although $p_{Z_{\mathrm{ext}}}^{(q)}(z;\mathbf{x})$, $q=1,2,\cdots,N_{\mathrm{R}}$ have been already obtained in the PDEM-based dynamic reliability analysis at $\mathbf{x}$, the increments, $D^{(q)}$, $q=1,2,\cdots,N_{\mathrm{R}}$, remain to be determined. Thus, the number of structural analyses involved in Eq.(28) or (29) is still N_{R}. Therefore, the same number of structural dynamic analyses are involved in the full and approximate dynamic reliability assessments.

3.3. Important Representative Points

To reduce the number of structural analyses in the approximate dynamic reliability assessment, the concepts of important representative regions (IRRs) and important representative points (IRPs) [32] are introduced.

In the context of the PDEM, the representative points are highly scattered in the probability space to reduce the discrepancy of the point set and consequently the numerical error in a global sense [40]. Nevertheless, only the representative points/regions which are adjacent to the limit state surface in the probability space have relatively large influence on the first-passage probability [41]. Specifically, for a representative point/region that is far from the limit state surface, the value of $p_{Z_{\mathrm{ext}}}^{(q)}(z;\mathbf{x})$ is generally small around $z=1$. Since $D^{(q)}$ is also small when a small perturbation $\mathbf{\Delta}$ is considered, for a representative point/region which is far from the limit state surface, the value of the integral of $p_{Z_{\mathrm{ext}}}^{(q)}(z;\mathbf{x})$ over $[1-D^{(q)},1]$ will be negligible. This feature allows to consider only a subset of the representative points/regions when evaluating Eq. (28) or (29).

Clearly, the greater is the value of $p_{Z_{\mathrm{ext}}}^{(q)}(z;\mathbf{x})$ at $z=1$, the greater impact $\mathbf{\theta}_q$ and V_q have on $\widehat{P_{\mathrm{F}}}(\mathbf{x}+\mathbf{\Delta})$. For numerical implementation, a screening parameter η is first introduced. Based on this parameter, if the inequality

$$p_{Z_{\mathrm{ext}}}^{(q)}(z=1;\mathbf{x}) \geq \eta \tag{30}$$

holds, the corresponding representative point, $\mathbf{\theta}_q$, and representative region, V_q, are selected as IRP and IRR, respectively. The sets of IRPs and IRRs are denoted by $\{\mathbf{\theta}_r^{\mathrm{IR}}\}_{r=1}^{N_{\mathrm{IR}}}$ and $\{V_r^{\mathrm{IR}}\}_{r=1}^{N_{\mathrm{IR}}}$, respectively. Besides, the assigned probabilities of the IRPs are denoted by $\{P_r^{\mathrm{IR}}\}_{r=1}^{N_{\mathrm{IR}}}$. Clearly, if the value of η increases, the number of IRPs will decrease, and when the screening parameter equals to 0, all representative points will be included in the set of IRPs, that is, $N_{\mathrm{IR}} = N_{\mathrm{R}}$.

If only the IRPs and IRRs are considered in Eq.(29), the approximate first-passage probability $\widehat{P_{\mathrm{F}}}(\mathbf{x}+\mathbf{\Delta})$ is given by

$$\widehat{P_{\mathrm{F}}}(\mathbf{x}+\mathbf{\Delta}) = P_{\mathrm{F}}(\mathbf{x}) + \sum_{q\in I_{\mathrm{IR}}} \int_{1-D^{(q)}}^{1} p_{Z_{\mathrm{ext}}}^{(q)}(z;\mathbf{x})\,\mathrm{d}z \tag{31}$$

where I_{RP} is the set of indexes of the important representative points. Thus, the parameter η controls the accuracy of the estimate and the associated computational efforts. Some practical guidelines for selecting the parameter eta are discussed in Section 5.1.

4. Sensitivity Analysis of First-Passage Probability

4.1. Approximate Sensitivity Estimation Based on IRPs

In order to solve the DRBTO problem with a first-order optimizer, the gradients of the objective and constraint functions are required. In general, the evaluation of first-order derivatives of reliability measures in the context of stochastic structural systems represents a challenging task from the numerical viewpoint. In this section, the sensitivity of the first-passage probability with respect to the design variables is derived based on the approximation formulated in Eq.(31).

By introducing a perturbation $\boldsymbol{\Delta}=(\mathit{\Delta}_1,\mathit{\Delta}_2,\cdots,\mathit{\Delta}_n)^{\mathsf{T}}$ to the design vector, the sensitivity of the first-passage probability with respect to the e-th design variable at $\mathbf{x}^\star$ is rewritten as

$$\left.\frac{\partial P_{\mathrm{F}}(\mathbf{x})}{\partial x_e}\right|_{\mathbf{x}=\mathbf{x}^\star}=\left.\frac{\partial P_{\mathrm{F}}(\mathbf{x}^\star+\boldsymbol{\Delta})}{\partial \mathit{\Delta}_e}\right|_{\boldsymbol{\Delta}=\mathbf{0}} \tag{32}$$

Replacing Eq.(31) into Eq.(32) yields an estimate of the sensitivity:

$$\left.\frac{\partial \widehat{P_{\mathrm{F}}}(\mathbf{x})}{\partial x_e}\right|_{\mathbf{x}=\mathbf{x}^\star}=\sum_{q\in I_{\mathrm{IR}}}\left[\frac{\partial}{\partial \mathit{\Delta}_e}\int_{1-D^{(q)}}^{1}p_{Z_{\mathrm{ext}}}^{(q)}(z;\mathbf{x}^\star)\,\mathrm{d}z\right]\Bigg|_{\boldsymbol{\Delta}=\mathbf{0}} \tag{33}$$

Next, define an auxiliary function:

$$\varphi^{(q)}(b)=\int_{-\infty}^{b}p_{Z_{\mathrm{ext}}}^{(q)}(z;\mathbf{x}^\star)\,\mathrm{d}z \tag{34}$$

then

$$\int_{1-D^{(q)}}^{1}p_{Z_{\mathrm{ext}}}^{(q)}(z;\mathbf{x}^\star)\,\mathrm{d}z=\varphi^{(q)}(1)-\varphi^{(q)}(1-D^{(q)}) \tag{35}$$

Since $\varphi^{(q)}(1)$ is a constant, differentiating Eq.(35) with respect to $\mathit{\Delta}_e$ at $\boldsymbol{\Delta}=0$ yields

$$\begin{aligned}\left[\frac{\partial}{\partial \mathit{\Delta}_e}\int_{1-D^{(q)}}^{1}p_{Z_{\mathrm{ext}}}^{(q)}(z;\mathbf{x}^\star)\,\mathrm{d}z\right]\Bigg|_{\boldsymbol{\Delta}=0}&=-\left[\frac{\partial}{\partial \mathit{\Delta}_e}\varphi^{(q)}(1-D^{(q)})\right]\Bigg|_{\boldsymbol{\Delta}=0}\\&=-\left.\frac{\partial\varphi^{(q)}(b)}{\partial b}\frac{\partial b}{\partial \mathit{\Delta}_e}\right|_{\substack{\boldsymbol{\Delta}=0\\ b=1-D^{(q)}}}\end{aligned} \tag{36}$$

where $D^{(q)}$ is equal to $D(\boldsymbol{\theta}_q,\mathbf{x},\boldsymbol{\Delta})$. From Eqs. (23) and (25), it is noted that if $\boldsymbol{\Delta}=\mathbf{0}$, $D^{(q)}$ is also zero. Thus, Eq.(36) is reformulated as

$$\left[\frac{\partial}{\partial \mathit{\Delta}_e}\int_{1-D^{(q)}}^{1}p_{Z_{\mathrm{ext}}}^{(q)}(z;\mathbf{x}^\star)\,\mathrm{d}z\right]\Bigg|_{\boldsymbol{\Delta}=0}=p_{Z_{\mathrm{ext}}}^{(q)}(z=1;\mathbf{x}^\star)\left.\frac{\partial Z_{\mathrm{ext}}(\boldsymbol{\theta}_q;\mathbf{x}^\star+\boldsymbol{\Delta})}{\partial \mathit{\Delta}_e}\right|_{\boldsymbol{\Delta}=\mathbf{0}} \tag{37}$$

By combining Eq.(33) and Eq.(37), the estimate of the sensitivity of the first-passage probability is obtained:

$$\left.\frac{\partial \widehat{P_{\mathrm{F}}}(\mathbf{x})}{\partial x_e}\right|_{\mathbf{x}=\mathbf{x}^\star}=\sum_{q\in I_{\mathrm{IR}}}p_{Z_{\mathrm{ext}}}^{(q)}(z=1;\mathbf{x}^\star)\left.\frac{\partial Z_{\mathrm{ext}}(\boldsymbol{\theta}_q;\mathbf{x})}{\partial x_e}\right|_{\mathbf{x}=\mathbf{x}^\star} \tag{38}$$

4.2. Sensitivity Evaluation of Extreme Response Function

Note that Eq.(38) involves the partial derivative of the normalized extreme value of the structural response. For numerical implementation, the normalized extreme value function in Eq.(8) can be replaced by a differentiable approximation, such as the normalized structural response at the peak time [42] or an aggregation function of the normalized structural response [5, 43]. In the present work, the nondifferentiable property of the normalized extreme value function is circumvented by using a class of aggregation function. In particular, the p-norm function

$$\widehat{Z_{\text{ext}}}\left(\boldsymbol{\theta}_q;\mathbf{x}\right)=\left(\sum_{j=1}^{N_{\mathrm{T}}}\left(\frac{Z\left(\boldsymbol{\theta}_q,t_j;\mathbf{x}\right)}{z^{\text{th}}}\right)^{\psi}\right)^{1/\psi} \tag{39}$$

is employed for sensitivity purposes, where $\widehat{Z_{\text{ext}}}$ is a smooth approximation of Z_{ext}; N_{T} is the number of time steps in the structural dynamic analysis; t_j denotes the j-th discrete time instant, i.e., $t_j = jh$; and ψ is the aggregation parameter. Note that the p-norm function is exactly the normalized extreme value function when $\psi \to +\infty$. To capture the extreme value of the structural response of interest, and avoid its nondifferentiability, an appropriate aggregation parameter value is selected. In particular, the aggregation parameter is set as 16 in the present implementation [43].

Note that the PDEM-based dynamic reliability analysis do not require the extreme value function to be differentiable. Therefore, the p-norm function is used instead of the extreme value function for the purpose of sensitivity analysis. Furthermore, the exact extreme value function is also used in the approximate reliability analysis as presented in Section 3.3. In other words, using the p-norm function instead of the extreme value function do not introduce errors into the reliability objective function or the reliability constraint function.

The sensitivity analysis of structural responses is a crucial subject in the field of structural optimization. Therefore, a large number of researches have been carried out for response sensitivity analysis. In this regard, the finite different method (FDM), the direct differentiation method (DDM) [44, 45], the adjoint method [46] and the semi-analytical method [47] have been developed to calculate the sensitivity of static and transient responses of linear and nonlinear systems. In this work, an adjoint method is employed to compute the partial derivative of Eq.(39). A detailed description of the adjoint method, which is based on a discretized formulation of the Newmark-β method, is provided in Appendix II. It is noted that the adjoint method is more efficient than the FDM and the DDM for sensitivity analysis, especially when a large number of design variables are considered. Therefore, the adjoint method is particularly favorable in topology optimization.

In Section 4.1, no restraints have been imposed on the type of the structures. In other words, the sensitivity estimate given by Eq. (38) can be used for both linear and nonlinear structures. Since the present work focuses on the topology optimization of linear structures, the adjoint method described in Appendix II is used only for linear systems. By introducing other methods for transient response sensitivity analysis of nonlinear systems, the proposed method can be extended to topology optimization of nonlinear structures.

5. Implementation Aspects

5.1. Reliability and Sensitivity Analysis

Regarding the accuracy of the reliability estimates, an upper bound of the error in the context of the PDEM has been provided in [40, 48]. This upper bound is given by the product of the discrepancy of the representative point set and the total variation of the function that characterizes the system. Noting that the total variation is an essential feature of the system, it cannot be changed. Therefore, the accuracy of the PDEM-based reliability analysis can be improved by reducing the discrepancy of the point set. The discrepancy of the representative point set is controlled by the number of representative points and the way how representative points are selected.

Thus, it is clear that the number of representative points, N_{R}, is a pivotal parameter in the PDEM-based dynamic reliability analysis. In fact, a number of factors, such as the dimensionality of the random vector $\boldsymbol{\Theta}$, the required accuracy of the reliability assessment, etc., have effect on the value of N_{R}. In general, a larger N_{R} will result in a lower discrepancy of the point set, and accordingly, a higher accuracy in the first-passage probability estimation. Note that a larger N_{R} will help to reduce the error in Eq.(25), which will also make the approximate first-passage probability in Eq.(31) and the approximate sensitivity in Eq.(37) more accurate. Nevertheless, more deterministic structural analyses have to be performed if a larger N_{R} is considered. In other words, N_{R} is determined by a trade-off between the numerical accuracy and the computational efforts. In the present implementation, an appropriate value of N_{R} is obtained by the GF-discrepancy minimization-based technique [49]. On the other hand, the presentative points are selected by a GF-discrepancy minimization-based approach as well (See Appendix I). These techniques are employed in the present work to ensure the accuracy of the PDEM-based reliability analysis.

In the context of dynamic reliability analysis (see Section 3.2) and sensitivity analysis (see Section 4), there are two approximations involved. The first one comes from Eq.(25), and it is controlled by the number of representative points. The second approximation is introduced by Eq.(30) where η is a crucial factor. Obviously, if $\eta = 0$, Eq.(31) will be identical to Eq.(29). In this case, there will be no reduction in computational efforts. On the other hand, a large value of η will lead to a nonnegligible error. Numerical experience indicates that setting η equal to a small positive value, e.g., $\eta = 0.001$, provides a reasonable tradeoff between accuracy and computational efforts, as shown in the numerical examples (see Section 6). It is noted that the strategy for selecting the IRP suggested in [32] can also be adopted in the proposed method. Based on this strategy, the IRPs are identified such that they account for a given percentage of the probability of failure. For details on this strategy, the reader can refer to [32].

Finally, it is noted that in principle, the out-crossing event-based method can also be used to estimate the first passage probability. However, since the transient responses of interest are not necessarily Gaussian for the type of problems under consideration, estimating the out-crossing rate is quite difficult. Therefore, this method is not suitable in the context of this work.

5.2. Optimization Procedure

Once the first-passage probability and its sensitivity are obtained, the DRBTO problems shown in Eqs.(10) and (11) can be solved by employing a first-order optimizer. In the present implementation, the method of moving asymptotes (MMA) [33] is adopted.

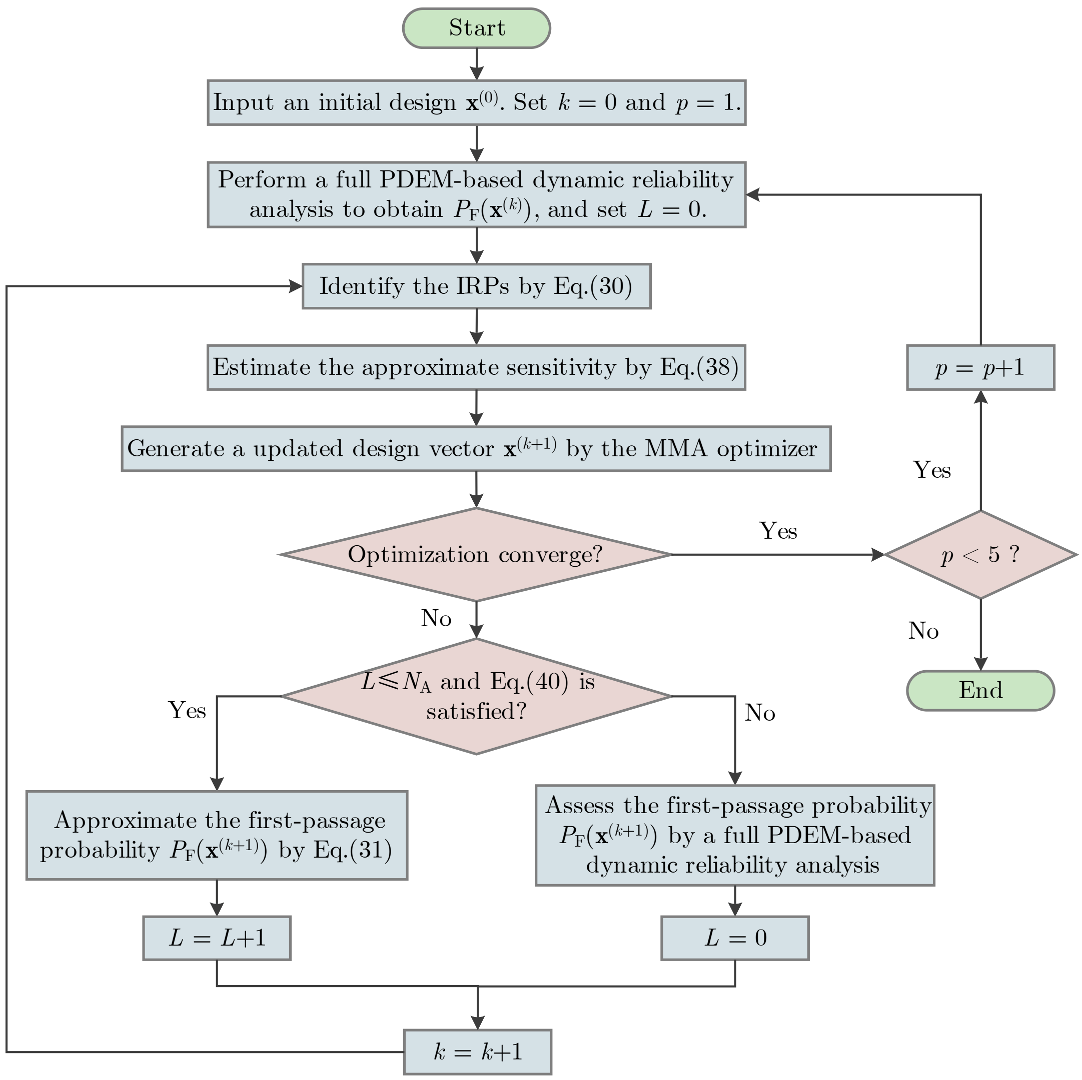

Fig. 2. Flowchart of the proposed method

During the optimization process, the first-passage probability has to be repetitively assessed. Therefore, the approximate dynamic reliability is employed to reduce the computation costs. Since the approximate formulation of the first-passage probability at $\mathbf{x}+\boldsymbol{\Delta}$ in Eq.(31) relies on the exact first-passage probability $P_{\mathrm{F}}(\mathbf{x})$, a heuristic strategy to switch between the full PDEM-based dynamic reliability assessment and the approximate dynamic reliability analysis is implemented. Assume that $P_{\mathrm{F}}\left(\mathbf{x}^{(k)}\right)$ is calculated by a full PDEM-based dynamic reliability analysis where $\mathbf{x}^{(k)}$ is the design vector at the k-th optimization iteration. If the design vector at the $(k+1)$-th iteration, i.e., $\mathbf{x}^{(k+1)}$, satisfies

$$\frac{\left\|\mathbf{x}^{(k+1)}-\mathbf{x}^{(k)}\right\|}{\left\|\mathbf{x}^{(k)}\right\|} \leq \epsilon \tag{40}$$

where ϵ is a small positive value and $\|\cdot\|$ denotes the 2-norm of a vector, then the approximate first-passage probability $\widehat{P_{\mathrm{F}}}\left(\mathbf{x}^{(k+1)}\right)$ is used instead of the exact one. Besides, to avoid accumulative errors in the first-passage probability assessment, at most N_A successive approximate dynamic reliability analyses are allowed. In the present implementation, $\epsilon=0.05$ and $N_A=5$. These values provide satisfactory results for the examples shown in Section 6.

Generally, the optimization problem, in the context of topology optimization, is nonconvex. Thus, first-order optimizers usually converge to local optima. Moreover, the value of the penalization parameter also has an effect on the convexity of topology optimization problems. For example, it has been pointed out that topology optimization problem that minimize the compliance is convex if $p=1$ [50]. However, an increase of the penalization factor, which is necessary for obtaining a binary design, will make the optimization problem nonconvex [51]. Furthermore, a larger value of the penalty factor will result in problems with higher nonconvexity. In this regard, the continuation approach has been developed to make the optimization problem well-posed while achieving a binary design [52]. Although the continuation approach is heuristic, it is suggested that this approach is able to alleviate the nonconvexity of the problem and has higher probability to find a global optimum [53].

The consideration of the first-passage probability in either the objective or constraint function makes DRBTO problems even more complicated than standard topology optimization problems. Therefore, to improve the robustness and convergence of the optimization process, a continuation variation on the SIMP model [53] is considered. The optimization problem is first solved with the penalization parameter $p=1$. Then the penalization parameter is increased by one, and the optimization problem is solved again with the previous solution as the initial design. This strategy is repeated until the penalization parameter reaches $p=5$. The corresponding flowchart of the proposed method is shown in Fig. 2.

Finally, it is noted that in principle, the proposed method can be applied to problems where random excitations are modeled by stochastic processes involving thousands of random variables. Nevertheless, the proposed method may loss its efficiency for this class of problems since the number of representative points will be large. A possible way to resolve this difficulty is to merge the proposed method into the framework of the globally-evolving-based generalized density evolution equation (GE-GDEE) [54], which is a new extension of the PDEM. This topic is a future research effort.

6. Case Studies

6.1. Structural Model

The thirty-story five-bay braced frame structure borrowed from Zhu et al. [35] is adopted to illustrate the effectiveness of the proposed method. In particular, the topology optimization of the lateral bracing system is considered. The corresponding ground structure is shown in Fig. 3.

The height of each floor is 4.572m and the width of each bay is 6.096m. Therefore, the total height and width of the structure is 137.160m and 30.480m, respectively. The structure is built with steel, so the density of the material is $\rho = 7800\,\mathrm{kg/m^3}$. All columns and beams in the structure are assigned with identical section attributes. Specifically, the area of the column/beam section, A_B, is $2.581\times10^{-2}\,\mathrm{m}^2$, and the moment of inertia of the column/beam section, I_B, is $1.665\times10^{-3}\,\mathrm{m}^4$. In addition, the section area of each brace, A_T, is $2.581\times10^{-2}\,\mathrm{m}^2$. The columns and the beams in the structure are modeled by 2D Euler-Bernoulli beam elements, while the braces are modeled by 2D truss elements. Thus, the finite element model of the ground structure includes 186 nodes, 330 beam elements, 300 truss elements and a total of 540 DOFs.

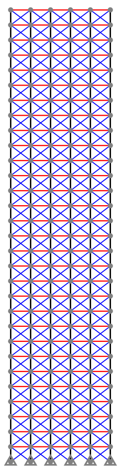

Fig. 3. Ground structure of the braced frame structure

To consider uncertainties in material properties, the Young's modulus of the structural members in floors 1~10, 11~20 and 21~30 are specified by three normally-distributed random variables, E_1, E_2

and E_3, respectively. Besides, nonstructural masses are also taken into account in the model. The additional masses in floors 1~10, 11~20 and 21~30 are characterized by three random variables, M_{A1}, M_{A2} and M_{A3}, respectively. These additional floor masses are considered by lumped masses uniformly distributed in the nodes of each floor, and they only influence the DOFs in the horizontal direction. The proportionality coefficients of the Rayleigh damping, i.e., a_0 and a_1, are set equal to 0.1641 and 0.0005, respectively.

Table 1. Probabilistic characterization of the random variables

Physical meaning	Floor	Random variable	Distribution type	Mean value	Coefficient of variation
Young's Modulus (10^{11} Pa)	1~10	E_1	Normal	2.1	0.05
	11~20	E_2	Normal	2.1	0.05
	21~30	E_3	Normal	2.1	0.05
Additional floor mass (10^4 kg)	1~10	M_{A1}	Normal	4.539	0.05
	11~20	M_{A2}	Normal	4.539	0.05
	21~30	M_{A3}	Normal	4.539	0.05
Combination coefficient (m/s^2)		A_1	Normal	0.2g	0.10
		A_2	Normal	0.2g	0.10

The braced frame structure is subjected to an earthquake excitation, which is modeled by a random combination of the normalized acceleration records of the El-Centro earthquake in the N-S and E-W directions:

$$\ddot{u}_g(A_1, A_2, t) = A_1 \ddot{u}_{g,\mathrm{NS}}(t) + A_2 \ddot{u}_{g,\mathrm{EW}}(t) \tag{41}$$

where A_1 and A_2 are the random combination coefficients; and $\ddot{u}_{g,\mathrm{NS}}$ and $\ddot{u}_{g,\mathrm{EW}}$ denote the normalized acceleration records of the El-Centro earthquake in the N-S and E-W directions, respectively.

The probabilistic characterizations of all random variables involved in the structural and excitation model are shown in Table 1, in which $\mathrm{g} = 9.807\,\mathrm{m}/\mathrm{s}^2$ denotes the acceleration of gravity. Note that the random variables are assumed to be normally-distributed for the purpose of demonstrating the efficacy of the proposed method. Clearly, the Young's Modulus and the additional floor mass should be positive from a physical point of view. Since the mean values of these random variables, which have small coefficients of variation, are far from zero, no truncation is necessary herein. For real-world engineering structures, the probabilistic characterization should be carefully determined such that physical constraints on structural parameters are satisfied.

6.2. Optimization of Outrigger Placement

6.2.1. Problem formulation

The core and outrigger structural system is a common structural configuration of high-rise buildings. The outriggers are horizontal structural components with large stiffness connecting the core and the outer columns to enhance the lateral stiffness [55]. Therefore, properly located outriggers can effectively reduce the horizontal deformation of a high-rise building. In this numerical example, the optimization of outrigger placement is considered.

The columns and beams remain invariant throughout the optimization process, while only the layout of the braces is optimized. The structure is assumed to have an X-braced core by retaining all braces in the third bay. In order to achieve the outrigger feature, all braces in each floor, except for those in the mid bay, are linked to a single design variable. As a result, the optimization problem involves 30 design variables, and each design variable controls the existence of eight brace members. Specifically, if the i-th design variable, x_i, is equal to one, all brace members in the i-th floor exist and they form an outrigger. In this way, the number of outriggers is interpreted as "material volume". Further, the constraint on the number of outriggers can be quantified by a volume constraint:

$$\mathbf{x}^{\mathsf{T}}\mathbf{v}_1 \le n_{\mathrm{O}} \tag{42}$$

where n_{O} is the allowed number of outriggers; and $\mathbf{v}_1$ is a 30-dimensional vector in which all elements are equal to one. The first-passage probability is defined in terms of the horizontal displacement of the rightmost node at the roof. If the horizontal displacement of interest exceeds the threshold, $z^{\mathrm{th}} = 0.8\mathrm{m}$, the structure is assumed to be failed. The objective of the optimization is to minimize the first-passage probability of the structure under the constraint on the number of outriggers. Consequently, the optimization problem is formulated as in Eq.(10).

Note that the roof displacement is selected herein only for the purpose of demonstration. Other structural responses can also be considered without any change in the method.

Since the dynamic reliability analysis is the foundation of DRBTO, a reliability validation is first carried out. The probability of failure, i.e., first-passage probability, of the optimized structure with one outrigger is assessed by the PDEM and MCS. In MCS (reference value), the number of samples is set equal to 10^5. In the PDEM, the number of the representative points is taken equal to 700. When only one outrigger is placed in the 14-th floor, the results obtained by the two methods are shown in Fig. 4. Note that this case corresponds to the solution of the optimization problem when only one outrigger is allowed (see Section 6.2.3). It is seen from the figure that the first-passage probability assessed by the PDEM is quite accurate compared with the one obtained by MCS. However, the number of structural dynamic analyses involved in the PDEM is much smaller, indicating that the PDEM is rather efficient in terms of the dynamic reliability analysis, as expected.

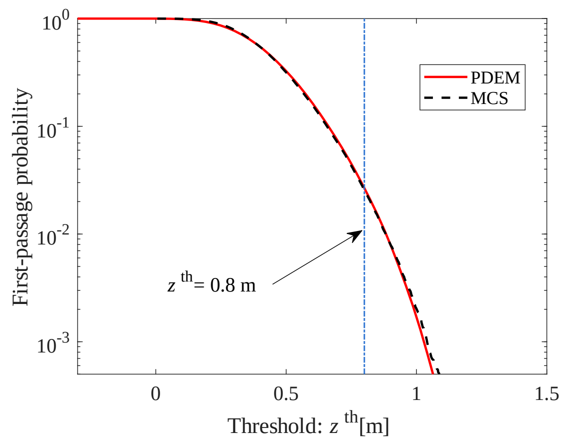

Fig. 4. Validation of the dynamic reliability analysis (one outrigger)

6.2.2. Sensitivity analysis

To assess the accuracy of the reliability sensitivity analysis technique implemented in the proposed approach, the sensitivity results obtained by different methods are compared in Fig. 5. These results correspond to the optimized structure with one outrigger (see Fig. 6 (a) in Section 6.2.3). In the figure, the method combining the full PDEM and the finite difference method (FDM), named PDEM-FDM, is considered as a reference. In other words, the PDEM-FDM estimates the reliability sensitivity by

$$\left.\frac{\partial P_{\mathrm{F}}(\mathbf{x})}{\partial x_e}\right|_{\mathbf{x}=\mathbf{x}^*} \approx \frac{P_{\mathrm{F}}(\mathbf{x}+\sigma\boldsymbol{\delta}_e)-P_{\mathrm{F}}(\mathbf{x})}{\sigma} \tag{43}$$

where σ is a step length, and $\boldsymbol{\delta}_e$ denotes a n-dimensional vector where all elements are zero except the e-th element which is equal to one. Note that both $P_{\mathrm{F}}(\mathbf{x})$ and $P_{\mathrm{F}}(\mathbf{x}+\sigma\boldsymbol{\delta}_e)$ are calculated by the full PDEM-based dynamic reliability analysis. Another reliability sensitivity analysis method, termed the PDEM-IRP-FDM and developed in [32], is adopted to compare the results with the proposed method. The PDEM-IRP-FDM also stems from Eq. (43) but employs the concept of IRP to enhance the efficiency. For numerical implementation, a screening parameter equal to 0.001 is selected, and the step length used in the finite difference method is set equal to 0.01. The closer the scatter points are to the diagonal (dashed line), the closer the sensitivity result is to the reference solution. It is observed that the sensitivity obtained by the proposed method is more accurate than the one obtained by the PDEM-IRP-FDM for this case.

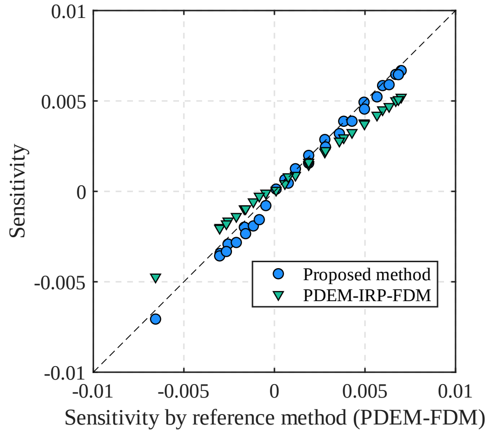

Fig. 5. Comparison of sensitivity analysis results obtained with different methods

In the full PDEM, 700 representative points are considered as indicated before. As a result, the total number of structural dynamic analyses required by the reference sensitivity analysis is 21000. In the PDEM-IRP-FDM, the number of considered IRPs is 35, and the resulting number of structural analyses involved in the sensitivity analysis is 1050. The number of IRPs identified in the proposed sensitivity analysis is 29. Therefore, only 29 adjoint problems (see Appendix II) are solved in the proposed sensitivity analysis. Note that the computational effort involved in solving the adjoint problem is similar to the one involved in a structural dynamic analysis. Thus, the proposed sensitivity analysis can accurately estimate the sensitivity of the first-passage probability with much lower computational costs than both the PDEM-FDM and the PDEM-IRP-FDM.

Although both the proposed method and the PDEM-IRP-FDM method are based on the concept of IRP, there are some differences in the criteria for sieving the IRPs. In fact, the PDEM-IRP-FDM is developed for general DRBDO problems where the structural analysis is treated as a black box. Therefore, the PDEM-IRP-FDM is based on a finite difference approximation to estimate the sensitivity of the first-passage probability [32]. On the contrary, the proposed method is developed on the basis of the adjoint method for transient response sensitivity analysis. These features lead to different criteria for selecting the IRPs and the resulting numbers of IRPs in the proposed method and the PDEM-IRP-FDM method. Besides, in order to obtain a stable estimate of the sensitivity of the first-passage probability, especially for nonlinear systems, a relatively large step length is required for the FDM in the PDEM-IRP-FDM. This feature of the PDEM-IRP-FDM can result in extra numerical errors in sensitivity evaluation, while the proposed method avoids this issue. Therefore, the proposed method presents higher accuracy than the PDEM-IRP-FDM. For a detailed description of the PDEM-IRP-FDM, the readers can refer to [32].

6.2.3. Optimization results

For illustration purposes, the reliability maximization problem is solved by the proposed method with different numbers of outriggers. For all cases, the full design, i.e., the design in which all design variables are equal to one, is used as the initial design. The optimized structures are shown in Fig. 6. When only a single outrigger is allowed, the outrigger is located in the 14-th floor, as shown in Fig. 6 (a). When two outriggers are considered, they are located in the 11-th and 15-th floors, respectively (see Fig. 6 (b)). As shown in Fig. 6 (c), the optimal locations include the 6-th, the 10-th and the 17-th floors if the permitted number of outriggers is three. The corresponding probabilities of failure of the three cases are 0.021, 0.013 and 0.005, respectively. Clearly, the probability of failure decreases when more outriggers are allowed, which is reasonable from a structural point of view.

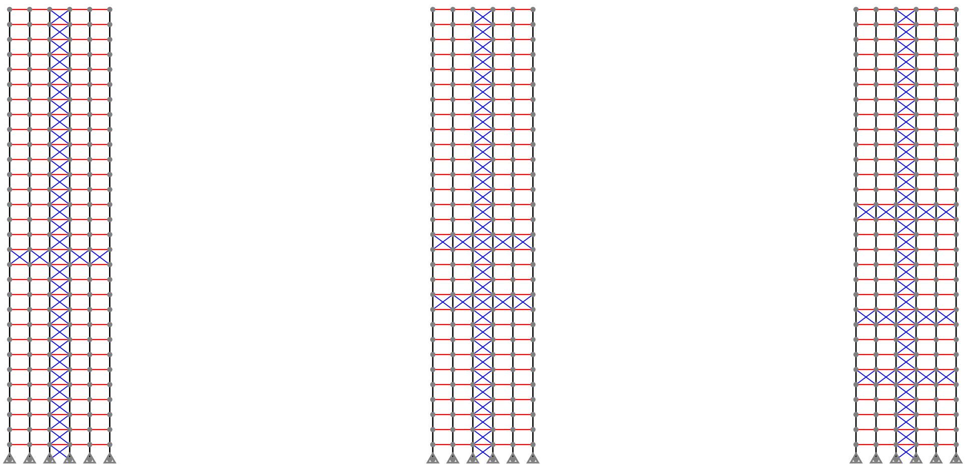

(a) One outrigger (b) Two outriggers (c) Three outriggers

Fig. 6. Optimized structures with different numbers of outriggers

As stated in Section 5.2, the optimization problem is repeatedly solved with different values of the penalization parameter p. Fig. 7 shows the values of the design variables obtained for different values of p, when a single outrigger is allowed. Three different initial designs are considered. Initial design 1 is the full design, where all design variables equals to one. In Initial designs 2 and 3, all design variables are set equal to a random number between zero and one, where a uniform distribution is assumed. It is observed that all cases converge to the same design. For all cases, when $p = 1$, almost all design variables attain relatively small values. As the value of p increases, the number of nonzero design variables decreases. When $p = 4$, there is only one nonzero design variable, namely, x_{14}, and the value of this design variable is identical to one, and therefore a binary design scheme is achieved. In fact, the optimization process converges at the stage when $p = 4$.

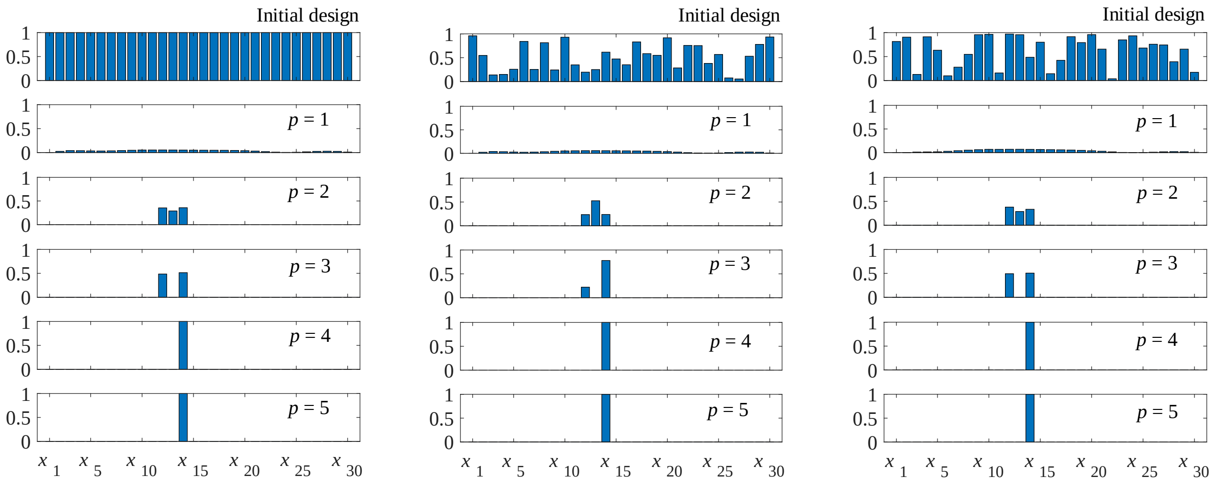

(a) Initial design 1 (b) Initial design 2 (c) Initial design 3

Fig. 7. Design variable values obtained after different optimization stages (one outrigger)

To get more insight into the proposed method, the outrigger placement optimization problem with one outrigger is also solved by the proposed method without the approximate dynamic reliability analysis introduced in Section 3.2 by setting $\eta = 0$. The iteration histories in terms of the value of the objective function, i.e., probability of failure, given by the proposed method without and with the approximate reliability analysis are presented in Fig. 8(a) and Fig. 8(b), respectively. While both cases converge to the same result, there are some differences between the iteration histories. It is seen that the optimization process without the approximate reliability analysis converges in less iterations. However, a full PDEM-based dynamic reliability analysis has to be carried out in each iteration, leading to about 150 full PDEM-based dynamic reliability analyses during the optimization process. Although more iterations are involved in the optimization process with approximate reliability analyses, only 39 full PDEM-based dynamic reliability analyses are conducted. Note that an approximate reliability assessment requires much less structural analyses than an exact one. Therefore, the approximate formulation outlined in Section 3.2 can reduce the computational efforts involved in the reliability analyses during the optimization process in a clear manner.

It is observed that jumps of the probability of failure values occur in Fig. 8 as the value of p is increased. The reason lies in the fact that, when the value of p is increased, the stiffness matrix of the structure controlled by intermediate design variables also changes drastically. During the initial stages of the optimization process, a number of design variables have intermediate values (see Fig. 7). As a result, the magnitude of the probability of failure jump is large. On the contrary, the values of the design variables approach zero or one during the last optimization stages. Thus, the magnitude of the jumps become small or even negligible. Similar interpretations of this phenomenon can also be found in [35].

To verify the optimization results obtained by the proposed method, the problem is solved graphically for the case when only one outrigger is considered. By placing the outrigger in each floor and then evaluating the objective function, Fig. 9 shows the values of the objective function associated with all feasible designs. It is observed that, when the outrigger is placed in the 14-floor, the objective function achieves its minimum. The result is consistent with the one obtained by the proposed method. Similar results are obtained when more outriggers are allowed. Since the outrigger placement optimization problem is constructed by the ground structure approach with the SIMP model, the real design space of this problem is a 30-dimensional hypercube. Thereby, the 30 designs presented in Fig. 9 is a set of vertex points in the real design space. Thus, Fig. 9 does not present the whole objective function space considered in the topology optimization problem, and therefore Fig. 9 cannot be used to assert the convexity of the optimization problem. Note that in general, verifying the convexity of a function in a high-dimensional space is a nontrivial task.

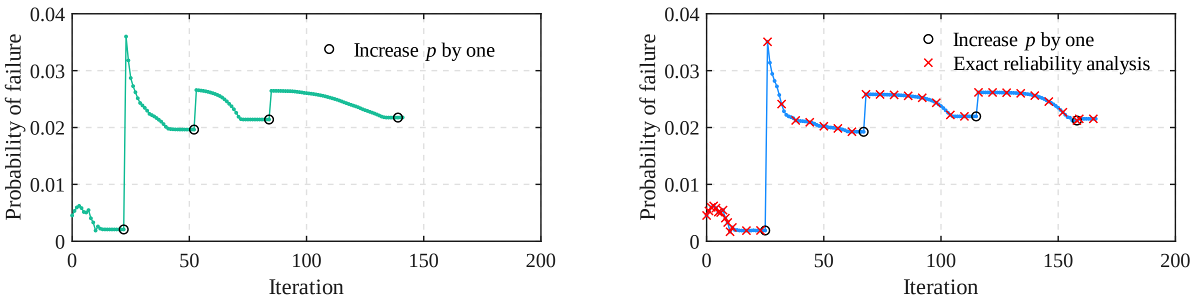

(a) Without approximate reliability analysis (b) With approximate reliability analysis

Fig. 8. Iteration history in terms of the value of the objective function (one outrigger)

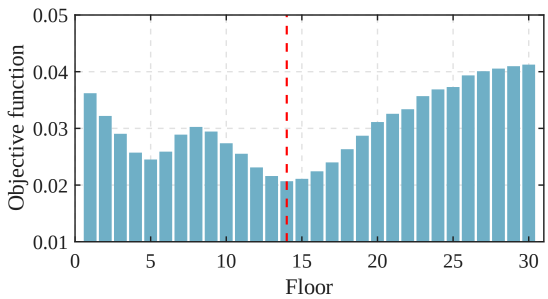

Fig. 9. Validation of the optimization result (one outrigger)

Finally, the number of IRPs identified by the proposed method in each optimization iteration is presented in Fig. 10, when two outriggers are allowed in the structure. It is seen that the number of IRPs is no more than 40 throughout the optimization process. Thereby, no more than 40 structural dynamic analyses (or adjoint analyses) are involved in the approximate dynamic reliability (or a sensitivity analysis of the first-passage probability). In fact, the maximum number of IRPs in the three cases considered in this section is less than 50. Noting that a full PDEM-based dynamic reliability analysis involves 700 structural analyses, the proposed method can considerably improve the efficiency of the solution of the previous DRBTO problem.

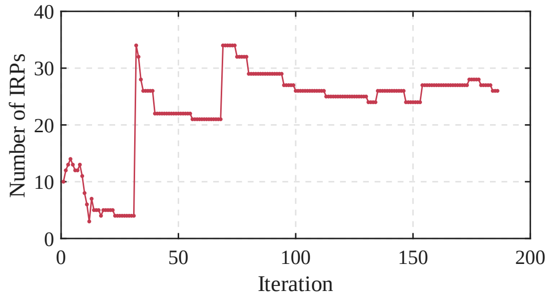

Fig. 10. Iteration history in terms of the number of IRPs (two outriggers)

As mentioned above, the value of η is determined empirically. The numerical results in this section show that $\eta = 0.001$ can provide a good trade-off between the computational costs and the numerical errors. To get more insight into the effect of η, the number of IRPs for different values of η is presented in Fig. 11. The results correspond the optimized structure with two outriggers. It is observed that, when the value of η is between 1×10^{-4} and 1×10^{-3}, the number of IRPs fluctuates within a narrow range. This result suggests that $\eta = 0.001$ is a reasonable choice for the proposed method.

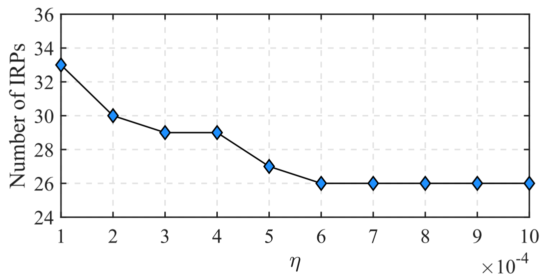

Fig. 11. Number of IRPs for different values of η (two outriggers)

6.3. Free-Form Topology Optimization of Braced System

In the second numerical example, a free-form topology optimization of the braced system is considered. The columns and beams remain invariant throughout the optimization process, while the braces are allowed to exist in a relatively independent manner. In particular, except for a symmetrical constraint on the horizontal direction, no other restriction is imposed on the form of the braced system. Thus, the number of design variables is 150, and each design variable controls the state of two brace components which are symmetrically distributed. As a result, the material volume measured by the number of braces is $\mathbf{x}^{\mathrm{T}}\mathbf{v}_2$, in which $\mathbf{v}_2$ is a 150-dimensional vector, of which each entry is equal to two.

The first-passage probability is defined in terms of the horizontal displacement of the rightmost node at the roof. If such displacement exceeds a prescribed threshold, z^{th}, the structure is assumed to be failed. In what follows, the two types of DRBTO problems presented in Section 2.3 are solved by the proposed method to evaluate its capabilities. In both cases, the number of representative points in a full PDEM-based reliability analysis is 700, and the screening parameter is equal to 0.001.

6.3.1. First-passage probability minimization problem

The first-passage probability is considered as the objective function and the material volume function is considered as the constraint function, as shown in Eq.(10). In all cases considered in this section, the design variables are set equal to one at the initial design.

(a) $\overline{v} = 20$ (b) $\overline{v} = 30$

Fig. 12. Optimized structure with different numbers of braces when $z^{\mathrm{th}} = 0.8\mathrm{m}$ (First-passage probability minimization problem)

The problem is solved by the proposed method with different values of the displacement threshold, z^{th}, and the maximum allowable material volume, $\overline{v}$. Fig. 12 shows the optimized structure for a threshold $z^{\mathrm{th}} = 0.8\mathrm{m}$ with allowed number of braces equal to 20 and 30. The first-passage probabilities of the optimized structures are 0.016 and 0.001, respectively. Clearly, the first-passage probability is smaller when more braces are included in the final design, which is consistent from a structural design point of view. Furthermore, it is noted that the brace layouts at the bottom sections of the two optimized structures show close affinity, while differences of the brace layouts are mainly observed at the middle sections of the two optimized structures. In addition, no braces are left at the top sections of both final designs. Thus, the braces at the bottom section of the frame structure are more significant in reducing the first-passage probability of the structure, which is anticipated.

(a) $\overline{v} = 30$ (b) $\overline{v} = 50$

Fig. 13. Optimized structure with different numbers of braces when $z^{\text{th}} = 0.6\text{m}$ (First-passage probability minimization problem)

Similarly to the previous figure, Fig. 13 shows the corresponding optimized structures for a threshold value $z^{\text{th}} = 0.6\text{m}$ and maximum allowed material $\overline{v} = 30$ and $\overline{v} = 50$. The optimization results are shown in (a) and (b), respectively. The first-passage probabilities associated with the optimized structures are 0.047 and 0.011, respectively. It is noted that, when the number of braces increases, the probability of failure, i.e., the first-passage probability, decreases. Besides, the braces at the bottom sections of the two optimized structures also show highly similar layouts, and in the case when $\overline{v} = 50$, more braces are placed at the middle and top sections of the structure. In addition, when the number of braces is 30, the probability of failure of the optimized structure with $z^{\text{th}} = 0.6\text{m}$ is larger than the probability of failure associated with case in which $z^{\text{th}} = 0.8\text{m}$, as expected. These features illustrate the consistency of the optimization results to some extent.

It is interesting to note that the probability of failure of the ground structure, i.e., the structure with all possible braces (300 braces), is 0.004 for a displacement threshold equal to 0.8m. This value is larger than the probability of failure of the structure shown in Fig. 12 (b), where only 30 braces are involved. This result reveals the fact that more unoptimized braces does not necessarily result in lower probability of failure. Clearly, the optimized structure can achieve higher reliability with less material consumption.

Therefore, the significance of performing DRBTO in the design of stochastic dynamical systems is evident.

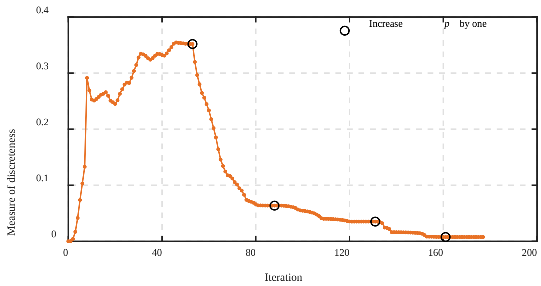

Fig. 14. Iteration history in terms of the measure of discreteness (First-passage probability minimization problem, $z^{\text{th}} = 0.8\text{m}$ and $\bar{v} = 30$)

To quantify the extent to which the different designs obtained during the optimization process are binary, a measure of discreteness is defined as [56]

$$M_{\mathrm{D}}(\mathbf{x}) = \frac{4\sum_{e=1}^{n} x_e (1 - x_e)}{n} \tag{44}$$

For a real binary design, the measure of discreteness is zero. For a design with lowest discreteness, i.e., the design in which all design variables are equal to 0.5, the measure of discreteness is one. The corresponding measure of all other cases is between zero and one. Evidently, the lower the value of the measure of discreteness is, the closer the design is to a binary design. Fig. 14 shows the iteration history in terms of the measure of discreteness for the case with displacement threshold $z^{\text{th}} = 0.8\text{m}$ and the allowable material volume $\bar{v} = 30$. Since a binary design, namely, the design corresponding to the ground structure, is adopted as the initial design, the measure of discreteness at the initial step is zero. The measure of discreteness keeps increasing during the stage with $p = 1$, which indicates that the optimization without penalty results in designs with a number of intermediate design variable values. By increasing the intensity of penalty, the measure is driven to a low level. At the last stage of the optimization process, the measure of discreteness is close to zero. Therefore, the optimization leads to a near-binary solution.

6.3.2. Material volume minimization problem

The material volume in terms of the number of braces is minimized subject to a constraint on the first-passage probability, as shown in Eq. (11).

The example is solved by the proposed method for two different displacement thresholds, namely,

$z^{\mathrm{th}} = 0.8\mathrm{m}$ and $z^{\mathrm{th}} = 0.6\mathrm{m}$. The full design is used as initial design for the two cases. The allowable probability of failure, $P_{\mathrm{F}}^{\mathrm{th}}$, is set as 0.01 in both the cases. The optimized structures are shown in Fig. 15. The number of brace members is 24 and 54 for threshold levels 0.8m and 0.6m, respectively.

Note that more braces are located in the bottom section of the structure as expected. Besides, no braces are placed at the top section of the structure as well. Compared with the structure obtained with $z^{\mathrm{th}} = 0.8\mathrm{m}$, more brace members are necessary for the case with $z^{\mathrm{th}} = 0.6\mathrm{m}$. This is reasonable from the engineering viewpoint, since stricter performance requirements are imposed in the latter case.

Fig. 16 shows the iteration history in terms of the probability of failure with displacement threshold $z^{\mathrm{th}} = 0.8\mathrm{m}$. It is seen that the optimization process converges when the penalization parameter p reaches 3 and that the probability of failure converges to 0.01. Thus, the constraint on the probability of failure is active at the final design.

(a) $z^{\mathrm{th}} = 0.8\mathrm{m}$ (b) $z^{\mathrm{th}} = 0.6\mathrm{m}$

Fig. 15. Optimized structures for different displacement thresholds (Material volume minimization problem)

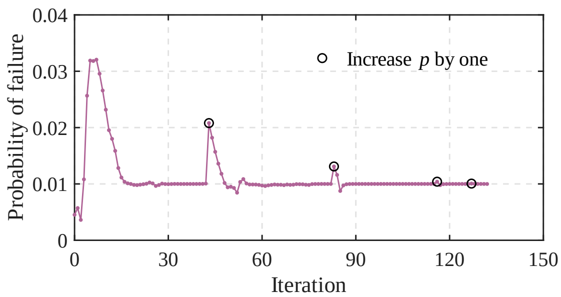

Fig. 16. Iteration history in terms of the probability of failure (Material volume minimization problem, $z^{\mathrm{th}} = 0.8\mathrm{m}$)

The number of brace members involved in the optimized structures and the corresponding probabilities of failure of all cases considered in Section 6.3 are listed in Table 2. The structures shown in Fig. 12 (a) and Fig. 12 (b) are obtained by solving the first-passage probability minimization problem, while the structures shown in Fig. 15 (a) are generated by solving the material volume minimization problem. Although the three structures are obtained by solving different optimization problems, the relationship between the number of braces and the probability of failure of the optimized structures follows a consistent trend. In particular, the number of remained braces in the structure obtained by minimizing the material volume is between the ones obtained in the two optimized structures which minimize the first-passage probability. Accordingly, the probability of failure of the structure in Fig. 15 (a) is also between the probabilities of failure of the two structures shown in Fig. 12. Similar trend can be observed in the three cases when $z^{\mathrm{th}} = 0.6\mathrm{m}$ is considered. Then, the optimization results obtained by the proposed method are reasonable from a qualitative point of view.

Table 2. Information of optimized structures for different cases

Optimized structure	Displacement threshold	Number of braces	Probability of failure
Fig. 12 (a)		20	0.016
Fig. 15 (a)	0.8m	24	0.010
Fig. 12 (b)		30	0.001
Fig. 13 (a)		30	0.047
Fig. 13 (b)	0.6m	50	0.011
Fig. 15 (b)		54	0.010

Finally, the effect of uncertainties on the reliability of the final designs is investigated. If all random variables are set equal to their mean values, the extreme value of the displacement of interest without braces is 0.39m. This value is lower than the two displacement thresholds considered in the present example. Thus, the frame structure without braces satisfies the displacement constraint under deterministic configurations. In other words, if no uncertainties are taken into account, no braces are necessary in the structure generated by topology optimization. However, the probabilities of failure of the frame structure without braces for $z^{\mathrm{th}} = 0.8\mathrm{m}$ and $z^{\mathrm{th}} = 0.6\mathrm{m}$ are 0.089 and 0.201, respectively. Clearly, the probability of failure of the structure obtained by deterministic topology optimization is unacceptably high. Therefore, the consideration of uncertainties in topology optimization is of great significance for ensuring the safety of the optimized structure.

7. Concluding Remarks

In the present paper, a method for dynamic-reliability-based topology optimization (DRBTO) is proposed. Both the first-passage probability minimization problem under material volume constraint and the material volume minimization problem under a single first-passage probability constraint are considered. To solve the DRBTO problems, the probability density evolution method (PDEM) is adopted to assess the first-passage probability. In addition, an approximate formulation of the first-passage probability at perturbed designs based on the important representative points (IRPs) is derived to enhance the efficiency of the repeated dynamic reliability analyses. The binary design variables are treated by the SIMP model. The sensitivity of the first-passage probability with respect to the design variables is estimated with the aid of the adjoint method and the approximate formulation of the first-passage probability. With the obtained first-passage probability and its sensitivity, the DRBTO problems are solved by the MMA optimizer. Finally, the effectiveness of the proposed method is illustrated by different DRBTO problems involving a braced frame structure. Some final remarks include:

(1) The PDEM is a foundation of the proposed method. The PDEM can be employed to assess the first-passage probability of linear or nonlinear stochastic systems under stationary or nonstationary excitations. Due to the generality of the PDEM, the proposed method has the potential of solving DRBTO problems of a number of stochastic dynamical systems in an efficient manner.

(2) Two different formulations of the DRBTO problem are considered in the present paper. The first one minimizes the probability of failure and the second one minimizes the material volume under the constraint on the probability of failure. Noting that the proposed method follows a standard optimization procedure, the optimization problem of both formulations can be solved in a similar manner.

(3) By introducing the concept of IRPs, an approximate formulation of the first-passage probability based on the PDEM is obtained. The approximate formulation can help to alleviate the computational efforts in the context of DRBTO without compromising the accuracy of the results.

(4) A relationship between the sensitivity of the first-passage probability and the transient response is enabled by virtue of the approximate failure probability formulation. By integrating the adjoint sensitivity analysis of transient responses, the sensitivities of the first-passage probability with respect to the design variables can be efficiently estimated. This allows the implementation of a first-order optimizer with reduced computational costs.

(5) The results of the example problems indicate that the proposed method represents a practical and useful numerical tool for the solution of a class of optimization problems.

Future research efforts include the consideration of more complex stochastic excitation models, for example, models characterized by thousands of random variables, and the application of the proposed method to structures with nonlinearity. The extension of the proposed method to the topology optimization of continuum structures represents another potential research direction.

Acknowledgements

The financial support from the National Natural Science Foundation of China (the National Distinguished Youth Fund of NSFC with Grant No. 51725804 and the NSFC-Guangdong Province Joint Project Grant No. U1711264) is highly appreciated. The financial support from CONICYT (National Commission for Scientific and Technological Research) under Grant No. 1200087 is also acknowledged. In addition, the financial support from China Scholarship Council (CSC) is gratefully appreciated by the first author.

Appendix I: Procedure of the PDEM-based dynamic reliability analysis

A general and brief numerical procedure for the PDEM-based dynamic reliability analysis is summarized as follows:

Step I.1: The probability space $\Omega_{\boldsymbol{\Theta}}$ is partitioned, and a set of representative points are selected [39]. The representative point set is selected by a GF-discrepancy minimization-based approach [40, 48]. The number of the representative points is also determined with the aid of the GF-discrepancy [49]. Denote the representative point set by $\{\boldsymbol{\theta}_q\}_{q=1}^{N_\mathrm{R}}$, in which $\boldsymbol{\theta}_q = (\theta_1, \theta_2, \cdots, \theta_N)^\mathsf{T}$ is the q-th representative point, and N_R is the total number of representative points. The assigned probability of $\boldsymbol{\theta}_q$ is defined as

$$P_q = \int_{V_q} p_{\boldsymbol{\Theta}}(\boldsymbol{\theta}) \mathrm{d}\boldsymbol{\theta} \tag{45}$$

where V_q is the representative region of $\boldsymbol{\theta}_q$ and it is characterized by a Voronoi cell. For more details about the GF-discrepancy and the point selection strategy, readers can refer to Chen and Chan [40].

Step I.2: Carry out the deterministic structural analysis at each representative point, namely, $\boldsymbol{\Theta} = \boldsymbol{\theta}_q$, $q = 1, 2, \cdots, N_\mathrm{R}$ by the Newmark-β method. The structural response of interest, $Z(\boldsymbol{\theta}_q, t; \mathbf{x})$, and consequently its normalized extreme value $Z_\mathrm{ext}(\boldsymbol{\theta}_q; \mathbf{x})$, are obtained. Then, the virtual stochastic process at each representative point, $W(\boldsymbol{\theta}_q, \tau; \mathbf{x})$, and its velocity process,

$\dot{W}(\boldsymbol{\theta}_q,\tau;\mathbf{x})$, are generated as indicated in Eq.(14).

Step I.3: For $q=1,2,\cdots,N_\mathrm{R}$, substitute $W(\boldsymbol{\theta}_q,\tau;\mathbf{x})$ with $W(\boldsymbol{\Theta},\tau;\mathbf{x})$ in the GDEE, i.e., Eq.(15), and a set of discretized GDEE are obtained:

$$\frac{\partial p_W^{(q)}(w,\tau;\mathbf{x})}{\partial \tau}+\dot{W}(\boldsymbol{\theta}_q,\tau;\mathbf{x})\frac{\partial p_W^{(q)}(w,\tau;\mathbf{x})}{\partial w}=0;\ q=1,2,\cdots,N_\mathrm{R} \tag{46}$$

where $p_W^{(q)}(w,\tau;\mathbf{x})=\int_{V_q} p_{W\boldsymbol{\Theta}}(w,\boldsymbol{\theta},\tau;\mathbf{x})\mathrm{d}\boldsymbol{\theta}$. Subsequently, the partial differential equations are solved by a finite difference method with total variation diminishing (TVD) scheme with the discretized initial condition $p_W^{(q)}(w,\tau;\mathbf{x})\big|_{\tau=0}=\delta(w)P_q$. For a detailed numerical scheme of the finite difference method, the readers are referred to Li and Chen [19].

Step I.4: Assess the PDF of the normalized extreme value of the structural response of interest by synthesizing the solutions of the GDEE at all representative points. In fact, the integral in Eq.(18) is calculated in the manner of summation:

$$p_{Z_\mathrm{ext}}(z;\mathbf{x})=\sum_{q=1}^{N_\mathrm{R}} p_{Z_\mathrm{ext}}^{(q)}(z;\mathbf{x}) \tag{47}$$

where $p_{Z_\mathrm{ext}}^{(q)}(z;\mathbf{x})=p_W^{(q)}(w=z,\tau=1;\mathbf{x})$, according to Eq.(17).

Step I.5: Finally, evaluating the one-dimensional integral in Eq.(19) by a numerical scheme, for instance, the trapezoidal rule, yields the first-passage probability.

Appendix II: Adjoint method for sensitivity analysis of structural response

The adjoint method is widely adopted in topology optimization, especially when structural analyses are time consuming. There are two different adjoint approaches for sensitivity analysis of dynamical structural systems [46], namely, the "differentiate-then-discretize" approach and "discretize-then-differentiate" approach. In this contribution, the "discretize-then-differentiate" approach [3, 57] is utilized.

Consider the dynamical system at a given representative point $\boldsymbol{\theta}_q$:

$$\mathbf{M}(\boldsymbol{\theta}_q;\mathbf{x})\ddot{\mathbf{Y}}+\mathbf{C}(\boldsymbol{\theta}_q;\mathbf{x})\dot{\mathbf{Y}}+\mathbf{K}(\boldsymbol{\theta}_q;\mathbf{x})\mathbf{Y}=\mathbf{f}(\boldsymbol{\theta}_q,t;\mathbf{x}) \tag{48}$$

of which the initial condition is

$$\mathbf{Y}(\boldsymbol{\theta}_q,t=0;\mathbf{x})=\mathbf{0};\ \dot{\mathbf{Y}}(\boldsymbol{\theta}_q,t=0;\mathbf{x})=\mathbf{0} \tag{49}$$

As previously pointed out, the Newmark-β method is used to solve the equation of motion. A discretized recurrence formula of the Newmark-β method is cast as [58]

$$\mathbf{R}\mathbf{Y}_{j+1}=\beta h^2\mathbf{f}_{j+1}+(0.5+\gamma-2\beta)h^2\mathbf{f}_j+(0.5-\gamma+\beta)h^2\mathbf{f}_{j-1}-\mathbf{P}\mathbf{Y}_j-\mathbf{Q}\mathbf{Y}_{j-1} \tag{50}$$

where h is a constant time step size; β and γ are two parameters in the Newmark-β method; $\mathbf{Y}_{j-1}$, $\mathbf{Y}_j$ and $\mathbf{Y}_{j+1}$ are the m-dimensional displacement vectors at time instants $t_{j-1}=(j-1)h$, $t_j = jh$ and $t_{j+1}=(j+1)h$, respectively; $\mathbf{f}_{j-1}$, $\mathbf{f}_j$, and $\mathbf{f}_{j+1}$ are the load vectors at time instants t_{j-1}, t_j and t_{j+1}; and the coefficient matrices, $\mathbf{R}$, $\mathbf{P}$ and $\mathbf{Q}$, are respectively defined as

$$\mathbf{R} = \mathbf{M} + \gamma h \mathbf{C} + \beta h^2 \mathbf{K} \tag{51}$$

$$\mathbf{P} = -2\mathbf{M} + (1-2\gamma) h \mathbf{C} + (0.5+\gamma-2\beta) h^2 \mathbf{K} \tag{52}$$

$$\mathbf{Q} = \mathbf{M} + (\gamma-1) h \mathbf{C} + (0.5-\gamma+\beta) h^2 \mathbf{K} \tag{53}$$

As mentioned previously in Section 2.2, a special case of the Newmark-β method, the constant average acceleration method is adopted. In other words, β and γ are set equal to 0.5 and 0.25, respectively.

Differentiating Eq.(50) with respect to design variable x_e yields

$$\begin{aligned} &\frac{\partial \mathbf{R}}{\partial x_e}\mathbf{Y}_{j+1} + \frac{\partial \mathbf{P}}{\partial x_e}\mathbf{Y}_{j} + \frac{\partial \mathbf{Q}}{\partial x_e}\mathbf{Y}_{j-1} + \mathbf{R}\frac{\partial \mathbf{Y}_{j+1}}{\partial x_e} + \mathbf{P}\frac{\partial \mathbf{Y}_{j}}{\partial x_e} + \mathbf{Q}\frac{\partial \mathbf{Y}_{j-1}}{\partial x_e} \\ &-\beta h^2 \frac{\partial \mathbf{f}_{j+1}}{\partial x_e} - (0.5+\gamma-2\beta) h^2 \frac{\partial \mathbf{f}_{j}}{\partial x_e} - (0.5-\gamma+\beta) h^2 \frac{\partial \mathbf{f}_{j-1}}{\partial x_e} = \mathbf{0} \end{aligned} \tag{54}$$

where

$$\frac{\partial \mathbf{R}}{\partial x_e} = \frac{\partial \mathbf{M}}{\partial x_e} + \gamma h \frac{\partial \mathbf{C}}{\partial x_e} + \beta h^2 \frac{\partial \mathbf{K}}{\partial x_e} \tag{55}$$

$$\frac{\partial \mathbf{P}}{\partial x_e} = -2\frac{\partial \mathbf{M}}{\partial x_e} + (1-2\gamma) h \frac{\partial \mathbf{C}}{\partial x_e} + (0.5+\gamma-2\beta) h^2 \frac{\partial \mathbf{K}}{\partial x_e} \tag{56}$$

$$\frac{\partial \mathbf{Q}}{\partial x_e} = \frac{\partial \mathbf{M}}{\partial x_e} + (\gamma-1) h \frac{\partial \mathbf{C}}{\partial x_e} + (0.5-\gamma+\beta) h^2 \frac{\partial \mathbf{K}}{\partial x_e} \tag{57}$$

As indicated in Section 2.2, the structural response of interest, Z, is a differentiable function of the displacement vector. Therefore, the sensitivity of the p-norm function in Eq.(39) with respect to design variable x_e is

$$\frac{\partial \widehat{Z_{\mathrm{ext}}}(\boldsymbol{\theta}_q;\mathbf{x})}{\partial x_e} = \frac{1}{z^{\mathrm{th}}}\left(\sum_{i=1}^{N_{\mathrm{T}}}(Z_i)^{\psi}\right)^{1/\psi-1} \sum_{j=1}^{N_{\mathrm{T}}}\left[(Z_j)^{\psi-1}\sum_{k=1}^{N_{\mathrm{T}}}\frac{\partial Z_j}{\partial \mathbf{Y}_k}\frac{\partial \mathbf{Y}_k}{\partial x_e}\right] \tag{58}$$

in which $Z_j = Z(\boldsymbol{\theta}_q, t_j; \mathbf{x})$. If Z is the displacement of the s-th DOF, i.e., $Z_j = Y_{j,s}$, where $Y_{j,s}$ is the s-th element of $\mathbf{Y}_j$, Eq.(58) is reduced to

$$\frac{\partial \widehat{Z_{\mathrm{ext}}}(\boldsymbol{\theta}_q;\mathbf{x})}{\partial x_e} = \frac{1}{z^{\mathrm{th}}}\left(\sum_{i=1}^{N_{\mathrm{T}}}(Y_{i,s})^{\psi}\right)^{1/\psi-1} \sum_{j=1}^{N_{\mathrm{T}}}\left[(Y_{j,s})^{\psi-1}\mathbf{e}_s^{\mathrm{T}}\frac{\partial \mathbf{Y}_j}{\partial x_e}\right] \tag{59}$$

where $\mathbf{e}_s$ is the s-th standard basis vector in an m-dimensional Euclidean space, whose all components are zero except the s-th component which is equal to one. By multiplying Eq.(54) by an m-dimensional adjoint vector $\boldsymbol{\lambda}_{N_{\mathrm{T}}-j+1}$ for $j = 1, 2, \cdots, N_{\mathrm{T}}$ and adding them to the right side of Eq.(59), the sensitivity is equivalently expressed as

$$\begin{aligned}\frac{\partial \widehat{Z_{\text{ext}}}(\boldsymbol{\theta}_q;\mathbf{x})}{\partial x_e} &= \sum_{j=1}^{N_{\mathrm{T}}}\left[c_j \mathbf{e}_s^{\mathsf{T}} \frac{\partial \mathbf{Y}_j}{\partial x_e} + \boldsymbol{\lambda}_{N_{\mathrm{T}}-j+1}^{\mathsf{T}}\left(\mathbf{R}\frac{\partial \mathbf{Y}_j}{\partial x_e} + \mathbf{P}\frac{\partial \mathbf{Y}_{j-1}}{\partial x_e} + \mathbf{Q}\frac{\partial \mathbf{Y}_{j-2}}{\partial x_e}\right)\right] \\ &+ \sum_{j=1}^{N_{\mathrm{T}}} \boldsymbol{\lambda}_{N_{\mathrm{T}}-j+1}^{\mathsf{T}}\left[\frac{\partial \mathbf{O}}{\partial x_e}\mathbf{Y}_j + \frac{\partial \mathbf{P}}{\partial x_e}\mathbf{Y}_{j-1} + \frac{\partial \mathbf{Q}}{\partial x_e}\mathbf{Y}_{j-2}\right] \\ &- \sum_{j=1}^{N_{\mathrm{T}}} \boldsymbol{\lambda}_{N_{\mathrm{T}}-j+1}^{\mathsf{T}}\left[\beta h^2 \frac{\partial \mathbf{f}_j}{\partial x_e} + (0.5+\gamma-2\beta)h^2 \frac{\partial \mathbf{f}_{j-1}}{\partial x_e} + (0.5-\gamma+\beta)h^2 \frac{\partial \mathbf{f}_{j-2}}{\partial x_e}\right]\end{aligned} \tag{60}$$

where

$$c_j = \frac{1}{z^{\text{th}}}\left(\sum_{i=1}^{N_{\mathrm{T}}}(Y_{i,s})^{\psi}\right)^{1/\psi-1}(Y_{j,s})^{\psi-1} \tag{61}$$

Noting that the initial condition in Eq.(49) is independent of the design vector, then $\partial \mathbf{Y}_0 \big/ \partial x_e = \mathbf{0}$. In Eq.(60), $\mathbf{Y}_{-1}$ and its gradient with respect to x_e are also required. In fact, $\mathbf{Y}_{-1}$ is computed by a central difference scheme using $\mathbf{Y}_0$ and $\dot{\mathbf{Y}}_0$ [3, 57]. Due to the initial condition given in Eq.(49), both, $\mathbf{Y}_{-1}$ and $\partial \mathbf{Y}_{-1} \big/ \partial x_e$ are zero vectors. In addition, both, $\partial \mathbf{f}_0 \big/ \partial x_e$ and $\partial \mathbf{f}_{-1} \big/ \partial x_e$ are zero vectors as well.

When the structure is subjected to earthquake excitations, the load vector is also a function of $\mathbf{x}$. According to Eq.(7), the partial derivative of the load vector is given by

$$\frac{\partial \mathbf{f}_j}{\partial x_e} = -\frac{\partial \mathbf{M}(\boldsymbol{\theta}_q, t; \mathbf{x})}{\partial x_e}\boldsymbol{\iota}\ddot{u}_g(\boldsymbol{\theta}_q, t) \tag{62}$$

To eliminate $\partial \mathbf{Y}_j \big/ \partial x_e$, $j = 1, 2, \cdots, N_{\mathrm{T}}$ from Eq.(60), the adjoint problem is derived as follows:

$$\begin{cases}\mathbf{R}\boldsymbol{\lambda}_1 = -c_{N_{\mathrm{T}}}\mathbf{e}_s^{\mathsf{T}} \\ \mathbf{R}\boldsymbol{\lambda}_2 + \mathbf{P}\boldsymbol{\lambda}_1 = -c_{N_{\mathrm{T}}-1}\mathbf{e}_s^{\mathsf{T}} \\ \mathbf{R}\boldsymbol{\lambda}_j + \mathbf{P}\boldsymbol{\lambda}_{j-1} + \mathbf{Q}\boldsymbol{\lambda}_{j-2} = -c_{N_{\mathrm{T}}-j+1}\mathbf{e}_s^{\mathsf{T}},\ j = 3, 4, \cdots, N_{\mathrm{T}}\end{cases} \tag{63}$$

By solving Eq.(63), the adjoint vectors, $\boldsymbol{\lambda}_j$, $j = 1, 2, \cdots, N_{\mathrm{T}}$, are obtained. Substituting $\boldsymbol{\lambda}_j$, $j = 1, 2, \cdots, N_{\mathrm{T}}$, into Eq.(60) gives the sensitivity:

$$\begin{aligned}\frac{\partial \widehat{Z_{\text{ext}}}(\boldsymbol{\theta}_q;\mathbf{x})}{\partial x_e} &= \sum_{j=1}^{N_{\mathrm{T}}} \boldsymbol{\lambda}_{N_{\mathrm{T}}-j+1}^{\mathsf{T}}\left[\frac{\partial \mathbf{R}}{\partial x_e}\mathbf{Y}_j + \frac{\partial \mathbf{P}}{\partial x_e}\mathbf{Y}_{j-1} + \frac{\partial \mathbf{Q}}{\partial x_e}\mathbf{Y}_{j-2}\right] \\ &- \sum_{j=1}^{N_{\mathrm{T}}} \boldsymbol{\lambda}_{N_{\mathrm{T}}-j+1}^{\mathsf{T}}\left[\beta h^2 \frac{\partial \mathbf{f}_j}{\partial x_e} + (0.5+\gamma-2\beta)h^2 \frac{\partial \mathbf{f}_{j-1}}{\partial x_e} + (0.5-\gamma+\beta)h^2 \frac{\partial \mathbf{f}_{j-2}}{\partial x_e}\right]\end{aligned} \tag{64}$$

It is noted that Eq.(63) consists of N_{T} systems of linear equations, and the size of each system is equal to the number of DOFs of the considered stochastic dynamical system, i.e., m. Therefore, the numerical cost for solving Eq.(63) is identical to the one associated with the solution of the equation of motion, Eq. (6), at a given realization of the random vector. In the adjoint method, Eq.(63) is solved once, while the FDM and the DDM need to solve the equation of motion n times. Noting that the number of design variables, i.e., n, is usually large in topology optimization, the adjoint method adopted herein is much more efficient than the FDM and the DDM. Thereby, the adjoint method is particularly suitable for topology optimization problems.

References

[1] Bendsøe MP, Sigmund O. Topology Optimization - Theory, Methods and Applications Berlin: Springer-Verlag; 2003.

[2] Sigmund O, Maute K. Topology optimization approaches - A comparative review. Structural and Multidisciplinary Optimization. 2013;48:1031-55.

[3] Le C, Bruns TE, Tortorelli DA. Material microstructure optimization for linear elastodynamic energy wave management. Journal of the Mechanics and Physics of Solids. 2012;60:351-78.

[4] Zargham S, Ward TA, Ramli R, Badruddin IA. Topology optimization: a review for structural designs under vibration problems. Structural and Multidisciplinary Optimization. 2016;53:1157-77.

[5] Zhao JP, Wang CJ. Topology optimization for minimizing the maximum dynamic response in the time domain using aggregation functional method. Computers & Structures. 2017;190:41-60.

[6] Ang AHS, Tang WH. Probability concepts in engineering: Emphasis on applications to civil and environmental engineering. 2nd Edition Hoboken: John Wiley & Sons; 2006.

[7] Kanno Y. On three concepts in robust design optimization: absolute robustness, relative robustness, and less variance. Structural and Multidisciplinary Optimization. 2020;62:979-1000.

[8] Chen SK, Chen W, Lee S. Level set based robust shape and topology optimization under random field uncertainties. Structural and Multidisciplinary Optimization. 2010;41:507-24.

[9] Asadpoure A, Tootkaboni M, Guest JK. Robust topology optimization of structures with uncertainties in stiffness – Application to truss structures. Computers & Structures. 2011;89:1131-41.

[10] Maute K, Frangopol DM. Reliability-based design of MEMS mechanisms by topology optimization. Computers & Structures. 2003;81:813-24.

[11] Mogami K, Nishiwaki S, Izui K, Yoshimura M, Kogiso N. Reliability-based structural optimization of frame structures for multiple failure criteria using topology optimization techniques. Structural and Multidisciplinary Optimization. 2006;32:299-311.

[12] Enevoldsen I, Sørensen JD. Reliability-based optimization in structural engineering. Structural Safety. 1994;15:169-96.

[13] Liang JH, Mourelatos ZP, Nikolaidis E. A single-loop approach for system reliability-based design optimization. Journal of Mechanical Design. 2007;129:1215-24.

[14] Du XP, Chen W. Sequential optimization and reliability assessment method for efficient probabilistic design. Journal of Mechanical Design. 2004;126:225-33.

[15] Chun J, Paulino GH, Song J. Reliability-based topology optimization by ground structure method employing a discrete filtering technique. Structural and Multidisciplinary Optimization. 2019;60:1035-58.

[16] Shen W, Ohsaki M, Yamakawa M. Quantile-based sequential optimization and reliability assessment for shape and topology optimization of plane frames using L-moments. Structural Safety. 2022;94:102153.

[17] Melchers RE, Beck AT. Structural Reliability Analysis and Prediction. 3rd Edition Hoboken: John Wiley & Sons; 2018.

[18] Jerez DJ, Jensen HA, Beer M. Reliability-based design optimization of structural systems under stochastic excitation: An overview. Mechanical Systems and Signal Processing. 2022;166:108397.

[19] Li J, Chen JB. Stochastic Dynamics of Structures Singapore: John Wiley & Sons; 2009.

[20] Crandall SH. First-crossing probabilities of the linear oscillator. Journal of Sound and Vibration. 1970;12:285-99.

[21] Iourtchenko D, Mo E, Naess A. Reliability of strongly nonlinear single degree of freedom dynamic systems by the path integration method. Journal of Applied Mechanics. 2008;75.

[22] Kougioumtzoglou IA, Spanos PD. Stochastic response analysis of the softening Duffing oscillator and ship capsizing probability determination via a numerical path integral approach. Probabilistic Engineering Mechanics. 2014;35:67-74.

[23] dos Santos KRM, Kougioumtzoglou IA, Spanos PD. Hilbert transform-based stochastic averaging technique for determining the survival probability of nonlinear oscillators. Journal of Engineering Mechanics. 2019;145:04019079.

[24] Xu B, Zhao L, Li WY, He JJ, Xie YM. Dynamic response reliability based topological optimization of continuum structures involving multi-phase materials. Composite Structures. 2016;149:134-44.

[25] Hu ZQ, Wang ZQ, Su C, Ma HT. Reliability based structural topology optimization considering non-stationary stochastic excitations. KSCE Journal of Civil Engineering. 2018;22:993-1001.

[26] Lutes LD, Sarkani S. Random Vibration: Analysis of Structural and Mechanical systems Burlington: Elsevier Butterworth-Heinemann; 2004.

[27] Chun J, Song J, Paulino GH. System-reliability-based design and topology optimization of structures under constraints on first-passage probability. Structural Safety. 2019;76:81-94.

[28] Bobby S, Suksuwan A, Spence SMJ, Kareem A. Reliability-based topology optimization of uncertain building systems subject to stochastic excitation. Structural Safety. 2017;66:1-16.

[29] Li J, Chen JB. Probability density evolution method for dynamic response analysis of structures with uncertain parameters. Computational Mechanics. 2004;34:400-9.

[30] Bendsøe MP. Optimal shape design as a material distribution problem. Structural optimization. 1989;1:193-202.

[31] Dorn W, Gomory R, Greenberg H. Automatic design of optimal structures. Journal de Mecanique. 1964;3:25-52.

[32] Yang JS, Chen JB, Jensen HA. Structural design optimization under dynamic reliability constraints based on the probability density evolution method and highly-efficient sensitivity analysis. Probabilistic Engineering Mechanics. 2022;68:103205.

[33] Svanberg K. The method of moving asymptotes—a new method for structural optimization. International Journal for Numerical Methods in Engineering. 1987;24:359-73.

[34] Xia Q, Wang MY, Shi T. A method for shape and topology optimization of truss-like structure. Structural and Multidisciplinary Optimization. 2013;47:687-97.

[35] Zhu M, Yang Y, Guest JK, Shields MD. Topology optimization for linear stationary stochastic dynamics: Applications to frame structures. Structural Safety. 2017;67:116-31.

[36] Chopra AK. Dynamics of Structures - Theory and Applications to Earthquake Engineering. 4th Edition Englewood Cliffs: Prentice Hall; 2012.

[37] Li J, Chen JB, Fan WL. The equivalent extreme-value event and evaluation of the structural system reliability. Structural Safety. 2007;29:112-31.

[38] Li J, Chen JB. The principle of preservation of probability and the generalized density evolution equation. Structural Safety. 2008;30:65-77.

[39] Chen JB, Ghanem R, Li J. Partition of the probability-assigned space in probability density evolution analysis of nonlinear stochastic structures. Probabilistic Engineering Mechanics. 2009;24:27-42.

[40] Chen JB, Chan JP. Error estimate of point selection in uncertainty quantification of nonlinear structures involving multiple nonuniformly distributed parameters. International Journal for Numerical Methods in

Engineering. 2019;118:536-60.

[41] Li LY, Papaioannou I, Straub D. Global reliability sensitivity estimation based on failure samples. Structural Safety. 2019;81:101871.

[42] Kang BS, Park GJ, Arora JS. A review of optimization of structures subjected to transient loads. Structural and Multidisciplinary Optimization. 2006;31:81-95.

[43] Gao WJ, Lu XL, Wang SS. Seismic topology optimization based on spectral approaches. Journal of Building Engineering. 2022;47:103781.

[44] Haukaas T, Der Kiureghian A. Parameter sensitivity and importance measures in nonlinear finite element reliability analysis. Journal of Engineering Mechanics. 2005;131:1013-26.

[45] Haukaas T, Scott MH. Shape sensitivities in the reliability analysis of nonlinear frame structures. Computers & Structures. 2006;84:964-77.

[46] Jensen JS, Nakshatrala PB, Tortorelli DA. On the consistency of adjoint sensitivity analysis for structural optimization of linear dynamic problems. Structural and Multidisciplinary Optimization. 2014;49:831-7.

[47] Fernandez F, Tortorelli DA. Semi-analytical sensitivity analysis for nonlinear transient problems. Structural and Multidisciplinary Optimization. 2018;58:2387-410.

[48] Chen JB, Yang JY, Li J. A GF-discrepancy for point selection in stochastic seismic response analysis of structures with uncertain parameters. Structural Safety. 2016;59:20-31.

[49] Chen JB, Yang JS, Jensen HA. Structural optimization considering dynamic reliability constraints via probability density evolution method and change of probability measure. Structural and Multidisciplinary Optimization. 2020;62:2499-516.

[50] Petersson J. On stiffness maximization of variable thickness sheet with unilateral contact. Quarterly of Applied Mathematics. 1996;54:541-50.

[51] Haber RB, Jog CS, Bendsøe MP. A new approach to variable-topology shape design using a constraint on perimeter. Structural Optimization. 1996;11:1-12.

[52] Sigmund O, Petersson J. Numerical instabilities in topology optimization: A survey on procedures dealing with checkerboards, mesh-dependencies and local minima. Structural Optimization. 1998;16:68-75.

[53] Stolpe M, Svanberg K. On the trajectories of penalization methods for topology optimization. Structural and Multidisciplinary Optimization. 2001;21:128-39.

[54] Lyu M-Z, Chen J-B. A unified formalism of the GE-GDEE for generic continuous responses and first-passage reliability analysis of multi-dimensional nonlinear systems subjected to non-white-noise excitations. Structural Safety. 2022;98:102233.

[55] Lee S, Tovar A. Outrigger placement in tall buildings using topology optimization. Engineering Structures. 2014;74:122-9.

[56] Sigmund O. Morphology-based black and white filters for topology optimization. Structural and Multidisciplinary Optimization. 2007;33:401-24.

[57] Chun J, Song J, Paulino GH. Structural topology optimization under constraints on instantaneous failure probability. Structural and Multidisciplinary Optimization. 2016;53:773-99.

[58] Chan SP, Cox HL, Benfield WA. Transient analysis of forced vibrations of complex structural-mechanical systems. The Journal of the Royal Aeronautical Society. 1962;66:457-60.